Genetic analysis of *Lamin A/C* gene variants in cases of sudden cardiac death admitted to a medico-legal laboratory

Submitted in partial fulfilment of the requirements for the MSc degree in Chemical Pathology, Faculty of Health Sciences, University of Pretoria

November 2022

Student:

Ms. Natalie Da Silva
U15091831
Department of Chemical Pathology
University of Pretoria
nataliadasilver@gmail.com

Supervisor:

Dr C van Niekerk
Principal Medical Scientist / Lecturer
Department of Chemical Pathology
University of Pretoria / NHLS
chantal.vanniekerk@up.ac.za

Co-supervisor:

Ms. B.S. van Deventer
Department of Forensic Medicine
Faculty of Health Sciences
University of Pretoria
barbara.vandeventer@yahoo.com

Head of Department:

Professor TS Pillay
Department of Chemical Pathology
University of Pretoria / NHLS
tahir.pillay@up.ac.za

Declaration of own work

I, the undersigned, hereby declare that this dissertation submitted to the University of Pretoria for the degree MSc (Chemical Pathology), and the work contained therein, is my own original work and has not previously, in its entirety or in part, been submitted to any university for a degree. Where previously published worked has been used, acknowledgement to the author(s) is provided in the reference list, which can be viewed at the end of this dissertation.

Signed:  on this day: 31st October 2022

Acknowledgements

"We must have perseverance and above all confidence in ourselves. We must believe that we are gifted for something and that this thing must be attained." – Marie Curie…

This quote sat above my bench throughout this entire project. I looked to it in moments of doubt and it reminded me of what I was given the opportunity to achieve. An achievement of which would not have been possible without the fantastic and inspiring individuals I mention here.

To my wonderful supervisor, Dr Chantel van Niekerk, I cannot express in words how your decision to take a chance on me in my honours year really changed the direction of my life. Without your continuous guidance and support, I would not have had the confidence in myself to complete this project. Thank you for believing in me and for allowing me to develop my skills as a scientist. Thank you for every kind word of encouragement and for always keeping calm when I thought I had broken something in the lab. I could not have achieved this without you and I will be forever grateful.

To Barbara, my fantastic co-supervisor. Thank you for always having a moment to chat with me, especially when I was uncertain of something. I appreciate you always going the extra mile for me and for taking time out of your own project to help me fix something or even just to check my spelling and numbering. It was a great pleasure to work with you over the last two years.

Lastly, to my darling family- my mother and father, my brother and my incredible partner, thank you for the endless support, love and care you have given me throughout this project. You were always there to listen to me ramble off about science things that didn't always make sense but you never complained and you always showed interest and fascination. I appreciate your patience and belief in me and for always telling me that I belong here and I will go on to do great things. Thank you for always providing a laugh when I needed one and for giving me a shoulder to cry on when I needed that too. I hope I have made you proud. I dedicate this project to you

and to God because without you all, I would not have been able to accomplish this. I love you all very much.

Table of Contents

List of Figures

List of Tables

List of Abbreviations

A

AF- Atrial fibrillation

AV- Atrio ventricular

AHA- American Heart Association

AIDS- Acquired immunodeficiency syndrome

Ala- Alanine

Asp- Aspartic Acid

AHRS- American Heart Rhythm Association

B

bp- Base pairs

BLAST- Basic Local Alignment Search Tool

C

C- Cytosine

CM- Cardiomyopathy

CAD- Coronary artery disease

CHD- Coronary heart disease

CVD- Cardiovascular disease

D

DCM- Dilated cardiomyopathy

DNA- Deoxyribonucleic acid

E

ECG- Echocardiogram

EDMD- Emery-Dreifuss muscular dystrophy

EDTA- Ethylenediaminetetraacetic acid

EHRS- European Heart Rhythm Society

EtBr- Ethidium Bromide

F

FDCM- Familial dilated cardiomyopathy

FPLD- Familial partial lipodystrophy

H

HF- Heart failure

HCM- Hypertrophic cardiomyopathy

HRM- High resolution melt

HIV- Human immunodeficiency virus

HGPS- Hutchinson-Guilford progeria syndrome

I

IC- Immune complex

IF- Intermediate filaments

Ig- Immunoglobulin

INM- Inner nuclear membrane

IDCM- Idiopathic dilated cardiomyopathy

K

Kb- Kilobases

L

LV- Left ventricular

LED- Light emitting diode

LHD- Lamin A/C heart disease

LGMD- Limb-girdle muscular dystrophy

LMNA-Lamin A/C

LMNB- Lamin B

M

Mass.- Massachusetts

mL- Milliliters

MLL- Medico-Legal Laboratory

Mo.- Missouri

N

N.J.- New Jersey

nm- Nanometers

NZ- New Zealand

NLS- Nuclear localization signal

NPC- Nuclear pore complex

NCBI- National Centre for Biotechnology Information

P

PCR-Polymerase chain reaction

PLN- Phospholamban

R

RCM- Restrictive cardiomyopathy

S

SA- South Africa

SD- Sudden death

SR- Sarcoplasmic reticulum

SCD- Sudden cardiac death

SNV- Single nucleotide variants

SSA- Sub-Saharan Africa

SUD- Sudden unexpected death

SCDY- Sudden cardiac death in the young

SUDI- Sudden unexpected death in infancy

SUDY- Sudden unexpected death in youth

T

T-Thymine

T_a- Annealing temperature

TAE- Tris-acetate- ethylenediaminetetraacetic acid

TNN- Titin

U

UK- United Kingdom

USA- United States of America

W

WHO- World Health Organization

List of Symbols

µL- Microliter

µM-Micromolar

pmol- Picomole

°C- Degrees Celsius

V- Volts

Abstract

The sudden death (SD) of a young and healthy individual can be traumatic. The incidence of SD in a young person is estimated to be between 1000 to 5000 people per year, globally. Approximately 85% of all SD cases are of cardiac origin, a condition known as sudden cardiac death (SCD).

Familial dilated cardiomyopathy (FDCM) accounts for a major portion of SCD cases. The pathogenesis of FDCM is associated with changes in the main components of the nuclear lamina, within cardiac myocytes. These components are termed lamins, and they are intermediate filament (IF) proteins encoded by the *Lamin A/C (LMNA)* gene. Causative variants of the *LMNA* gene are a major risk factor for lethal arrhythmias and SD. These pathogenic variants provide crucial prognostic value for diagnosis of FDCM and can be highly predictive for SCD.

This study aimed to identify variations in the *LMNA* gene among SCD cases, within a cohort representative of the South African population. Genomic deoxyribonucleic acid (DNA) was extracted from whole blood samples from 66 case subjects and nine controls. The extracted case and control DNA samples were subjected to real-time polymerase chain reaction (PCR) amplification followed by high-resolution melt (HRM) curve analysis. Samples were grouped according to their melt curve profile similarities and a representative sample from each group was sent for sequencing via automated Sanger sequencing. Sequencing results, in the form of chromatographs were analysed.

Following sequencing analysis, two single nucleotide variants (SNVs) were identified in both case and control samples. The SNVs c.861T>C; p.Ala287 (rs535089) and c.1338T>C; p.Asp446 (rs505058) are classified as synonymous variants as there are no changes in the resulting amino acids. Of the 66 case samples and nine control samples, 46 case samples and eight control samples harboured either one or both of the identified SNVs. Of these, 21 case samples and eight control samples carried only the SNV rs538089, 19 case samples and one control sample carried both SNVs, and six case samples carried only the SNV rs505058. As is common among *LMNA* genetic

variants, the majority of these SNVs carriers were males (71.7%) and of African descent (80.4%). Although previously classified as benign, these variants have been associated with dilated cardiomyopathy (DCM) and other laminopathy phenotypes such as Emery-Dreifuss muscular dystrophy (EDMD), limb-girdle muscular dystrophy (LGMD), Hutchinson-Guilford progeria syndrome (HGPS) and Charcot-Marie Tooth disorder. Within our study population, it was noted that in a case subject, whose cause of death was determined to be a SCD due to suspected DCM, both SNVs were detected.

This study sheds light on the need for further research into *LMNA* gene variants among the South African population. Due to their unique diagnostic value, inclusion of these variants in genetic screening panels can aid in confirming diagnosis of DCM and heart failure (HF), preventing SCD in young, otherwise healthy, individuals and further investigating other *LMNA*-associated diseases, which may arise as our population grows and diversifies.

Chapter 1: Literature Review

'Sudden death' or 'sudden unexpected death' (SUD) are terms used, interchangeably across all literature, to describe an unforeseen or instant death, which occurs in an otherwise healthy individual (Saadi *et al.*, 2020). Sudden death is common amongst the elderly, however, it is estimated that between 5000-7000 children and young adults die a SD, in the United States of America (USA), each year - leading to a significant societal burden (Fan *et al.*, 2022).

In South Africa (SA), a SD is defined as an unnatural death, in terms of the Regulations Regarding the Rendering of Forensic Pathology Services R636 and, therefore, is referred to a mandatory, medico-legal investigation (Inquests Act 58 of 1959), in order to determine possible cause of death. However, in a substantial number of SD cases in SA, the cause of death remains elusive after a full investigation (van Deventer *et al.*, 2016).

It is the consensus, across all the revised literature, that the majority of SD cases are as a result of underlying cardiovascular causes (Saadi *et al.*, 2020). Approximately, 30% to 40% of SD cases in the young (birth to 45 years) are due to an inherited cardiovascular disease (CVD), where death is often the first manifestation (Basso *et al.*, 2010; Saadi *et al.*, 2020). A global burden of disease study, reported by Shaboodien *et al.* (2020), claimed CVD is a major cause of mortality, globally, and is the second most frequent cause of death in Sub-Saharan Africa (SSA), following the human immunodeficiency virus/acquired immunodeficiency syndrome (HIV/AIDS). In 2017, CVD causes were found in 38% of all non-communicable disease-related deaths in Africa (Keates *et al.*, 2017). Considering that 35.7% of the South African population is aged 35 years or younger, SD due to undetected CVD can lead to a dramatic loss of economically active adults and a significant burden to an already overstretched health system.

1.1 Sudden cardiac death

It is reported that 70% of all SD cases are classified as SCDs (Fan *et al.*, 2022). Sudden cardiac deaths are defined as natural deaths due to underlying cardiac pathologies, preempted by an abrupt loss of consciousness, occurring within one hour after the severe and sudden onset of symptoms (Ferrero-Miliani *et al.*, 2010). Often, SCD cases occur as unobserved, out-of-hospital events.

There are challenges in determining the exact etiology of SCDs. Limited information exists due to a lack of uniform autopsy protocols, an inability to establish mandatory reporting requirements, and variances in case ascertainment procedures (D'Ascenzi *et al.*, 2022). Coronary heart diseases (CHDs) account for approximately 80% of SCD cases in middle-aged individuals (55 years and older) (Campuzano *et al.*, 2014). Vascular disorders of the myocardium, including acute myocardial infarction, are the dominant causes of SCD in older patients and are often regarded as the first expression of coronary artery disease (CAD) (Markwerth *et al.*, 2021).

Although a rare occurrence, SCD in childhood, adolescence, and early adulthood typically leads to an instant death (Markwerth *et al.*, 2021). In a recent prospective, population-based study conducted in Australia and New Zealand (NZ), Gray *et al.* (2019) stated the prevalence of sudden cardiac death in the youth (SCDY <45 years) as 1.3 cases per 100 000 persons, with males accounting for a majority of the deceased. Basso *et al.* (2010), reported that 30% to 40% of SCDY cases are due to genetic cardiac disorders. Inherited cardiac diseases, commonly associated with SCD in children and young adults, are grouped into genetic structural and non-structural pathologies (Fan *et al.*, 2022). Structural abnormalities of SCDY, which include cardiomyopathies (CM), myocarditis, premature CAD, and congenital heart disease, are typically identified during a routine gross and histopathological autopsy investigation (Gray *et al.*, 2019). However, in one-third of SCDY cases, a cause of death is not found, despite the completion of a comprehensive autopsy investigation accompanied by other auxiliary investigations, such as toxicology and histology (Bagnall *et al.*, 2016). These cases are termed unexplained SCDs. Unexplained SCDs

are described in the autopsy report as a death caused by a supposed cardiac arrhythmia (Sanchez *et al.*, 2016). These arrhythmias are secondary to underlying primary arrhythmogenic disorders, commonly termed 'channelopathies', which leave no evidence to be found during a comprehensive macroscopic post-mortem investigation (Gray *et al.*, 2019).

Despite the grouping of inherited cardiac diseases associated with SCDY, into two main groups (structural or non-structural), significant overlaps between the two groups have been reported (Campuzano *et al.*, 2014). For example, Sanchez *et al.* (2016) stated that CMs usually present with anatomo-morphological malformations in the cardiac tissue which can be found during autopsy examinations. However, Gray *et al.* (2019) report that despite no evidence of structural change at autopsy, CM may be clinically diagnosed, genetically (via molecular autopsy), or in a family, as lethal arrhythmias could precede any evidence of overt structural changes. Recent reports have emerged that suggest CM could be responsible for SCD in a structurally normal heart (Sanchez *et al.*, 2016)

1.2 Cardiomyopathies

Cardiomyopathies are a heterogeneous cluster of morpho-functional heart diseases (Seferović *et al.*, 2019). These diseases are associated with structural malformations of the cardiac tissue, which involve hypertrophy, and dilatation of fatty and/or fibrotic infiltration (Campuzano *et al.*, 2014). These abnormalities may be responsible for inducing life-threatening arrhythmias. The worldwide prevalence of CM is estimated at 2.5 million cases and is forecasted to increase within the next decade. In a South African hospital-based study, Shaboodien *et al.* (2020) reported the highest prevalence of CM in SSA, 40.2%. In approximately 10% of SCD cases, CM is defined as the cause of death (Ferrero-Miliani *et al.*, 2010). Cardiomyopathies are clinically classified as either familial/genetic or acquired. Genetically predisposed CM is predominantly inherited in an autosomal dominant pattern (Gray *et al.*, 2019). Four main forms of CMs are frequently described across all available literature.

Hypertrophic cardiomyopathy (HCM), a monogenetic disease, resulting from variations in the genes encoding sarcomere proteins (Shaboodien *et al.*, 2020). Hypertrophic cardiomyopathy is indicated by the thickening of the cardiac muscle tissue, with no exclusive ethnic, geographic, or gender distribution in the disease (Fan *et al.*, 2022). Although HCM has, historically, been considered rare among Africans, there is inadequate evidence regarding the reevaluation of incidence, genetics, and clinical outcomes of HCM on the African continent, today (Shaboodien *et al.*, 2020).

Arrhythmogenic right ventricular cardiomyopathy (ARVC/ARVM), dubbed the 'disease of the desmosome', is due to pathogenic variations in the genes encoding the desmosomal proteins of the intercalated disks, located between cardiomyocytes (Vimalanathan *et al.*, 2018). Also inherited in an autosomal dominant fashion, genetic penetrance of ARVC/ARVM is highly related to gender with a specific tendency in males (Ferrero-Miliani *et al.*, 2010). Arrhythmogenic right ventricular cardiomyopathy is indicated by advancing fibrofatty scar tissue, which progressively replaces the cardiomyocytes (figure 1), resulting in the thinning of the right (and in some cases, the left) ventricular walls (Fan *et al.*, 2022). This form of CM is often associated with SCD in young athletes as arduous physical activity can lead to cardiac arrhythmia (Vimalanathan *et al.*, 2018).

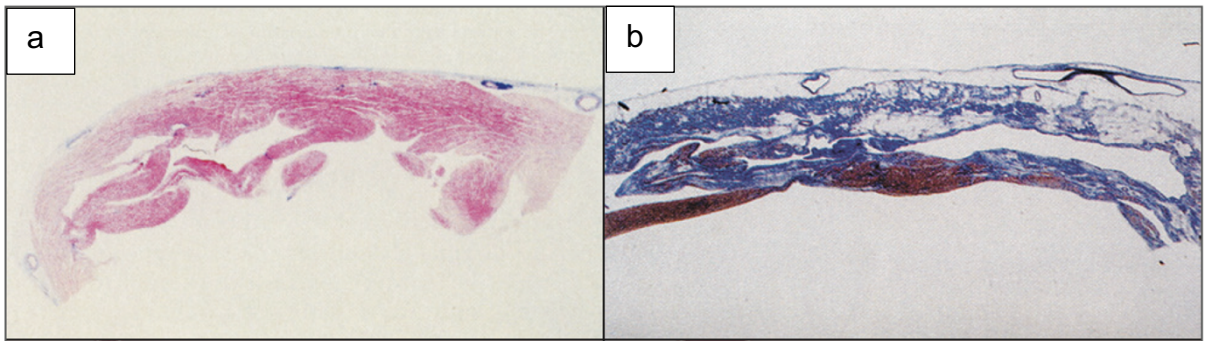

Figure 1 Comparing the right ventricular wall in a healthy individual **(a)** versus in an ARVC/ARVM patient **(b),** who died suddenly. When stained with azan trichrome, healthy cardiomyocytes appear red, fibrous tissue appears blue and fatty tissue appears white. Arrhythmogenic right ventricular cardiomyopathy is indicated by advancing replacement of cardiomyocytes by fibrous and fatty scar tissue (seen in b). This results in the thinning of the right ventricular wall, inducing arrhythmias (Corrado *et al.*, 2017).

Restrictive cardiomyopathy (RCM) is a lethal but rare disease, most commonly caused by infiltration and, in a smaller number of cases, by pathogenic genetic variants (Cimiotti *et al.*, 2021). This disease is indicated by nondilated left or right ventricles with diastolic dysfunction. It is a myocardial condition that results from advanced myocardial stiffness (Fan *et al.*, 2022). The most common causative variants, implicated in RCM, have been located in genes encoding the sarcomere proteins, however, recent studies have found other pathogenic variants in proteins that are not involved in the contraction and relaxation of cardiomyocytes (Cimiotti *et al.*, 2021).

Dilated cardiomyopathy is the most frequently genetically induced form of CM (Mohan *et al.*, 2002). This disease leads to HF, later progressing to multiple organ failure (Caviedes Bottner *et al.*, 2018). In Africa, DCM is implicated in 10% to 17% of all cardiac diseases diagnosed at autopsy and accounts for 17% to 48% of HF hospitalisations (Mayosi & Somers, 2007). Dilated cardiomyopathy has been implicated in a significant number of SCD cases (Fan *et al.*, 2022). Due to the high mortality rate, DCM is the main indication for cardiac transplantation in children and young adults (Caviedes Bottner *et al.*, 2018). It is estimated that 25% to 30% of all DCM cases have an identifiable familial component (Rosenbaum *et al.*, 2020). However, due to the lack of accepted diagnostic criteria, it is believed that the percentage of familial DCM cases may be higher than initially suspected (Japp *et al.*, 2016; Mohan *et al.*, 2002).

1.3 Familial dilated cardiomyopathy

The World Health Organization (WHO) defines DCM as a concerning cardiac disease in which structural or functional malformations of the cardiac muscle can result in significant morbidity and mortality, resulting in complications such as HF and arrhythmia (Jain *et al.*, 2021).

Dilated cardiomyopathy is a heterogenous disorder, with features of ventricular and, at times, atrial dilatation with normal or diminished wall thickness (Mohan *et al.*, 2002). The disease is usually indicated by a left-ventricular ejection fraction (LVEF) of less than 45% accompanied by left-ventricular (LV) end-diastolic dimensions of greater

than 112% (taking into account age and body surface area) (Rosenbaum *et al.*, 2020). During the initial stages of DCM LV alterations occur, as a protective response, to compensate for decreased contractility. However, as the disease progresses, the LV wall becomes dilated (figure 2a) and defective, steering toward progressive failure with peripheral hypoperfusion and retrograde failure with lung oedema and venous obstruction (figure 2b) (Caviedes Bottner *et al.*, 2018). Dilated cardiomyopathy can present as a primary disorder of myocardial dysfunction or in conjunction with a variety of cardiac and non-cardiac diseases (Peters *et al.*, 2020).

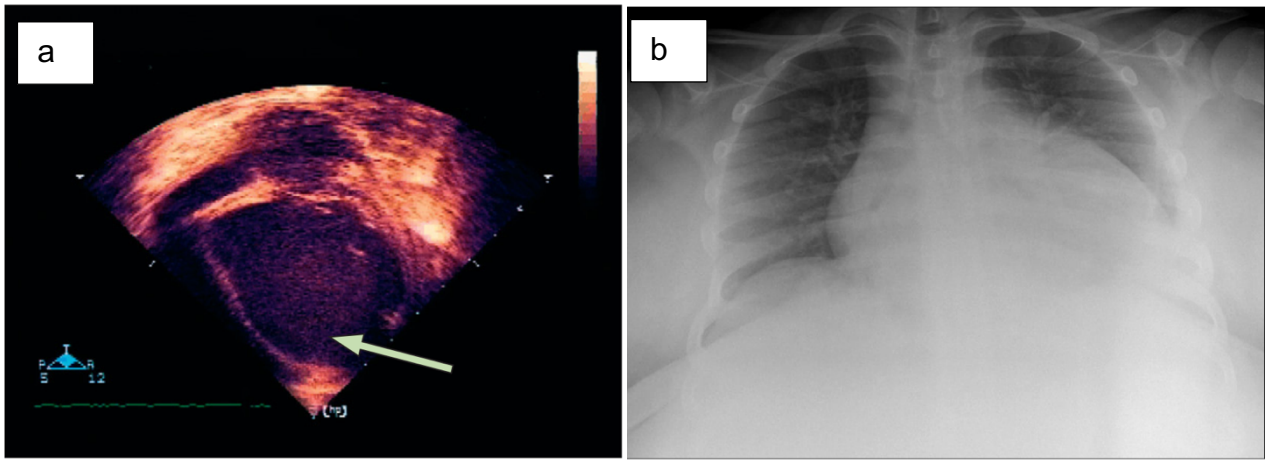

Figure 2(a) A transthoracic echocardiogram (ECG) of a DCM patient shows a dilated left ventricle (arrow), systolic function is severely hindered. **(b)** A chest radiograph of a DCM patient shows severe cardiomegaly and pulmonary oedema consistent with DCM (Jefferies & Towbin, 2010).

Dilated cardiomyopathy is common among younger children, and males and is specifically common among black individuals (Caviedes Bottner *et al.*, 2018). In an estimated 36% of all HF cases, DCM is found to be the root cause (Rosenbaum *et al.*, 2020). In a recent study reported by Seferović *et al.* (2019), 32% of patients with recent onset DCM presented with HF and 66% of patients had at least one previous HF hospitalisation before the commencement of the study. In SSA, FDCM accounts for 21.4% of all HF cases (Agbor *et al.*, 2018). Heart failure is a serious public health issue in Africa and SA, associated with high death rates and poor quality of life.

The American Heart Association (AHA) groups the causes of DCM into genetic/familial, mixed, or acquired (Jain *et al.*, 2021). The term 'mixed' is most commonly reserved for sporadic cases of DCM that may arise due to genetic-environmental interactions. Causes of DCM include persistent viral infections and activated autoantibodies and immune complexes (ICs), toxic damage caused by chemotherapy treatments and genetic variants that affect structural proteins (figure 3) (Jain *et al.*, 2021). Approximately, 70% of DCM cases are classified as 'idiopathic' DCM (IDCM) (Caviedes Bottner *et al.*, 2018). This diagnosis is made because no clear and identifiable cause of DCM was found in the patient during a routine autopsy (Jain *et al.*, 2021). However, IDCM diagnosis does not exclude genetic causes (Mohan *et al.*, 2002). It is reported that 20% to 50% of all IDCM cases are determined to be familial (Ferrero-Miliani *et al.*, 2010). Positive family history can be found in 30% to 35% of all DCM cases and a genetic factor can be detected in 40% of sporadic DCM patients (Seferović *et al.*, 2019). Familial DCM should be highly suspected if there is a positive family history of DCM in more than one family member and if a family member has experienced a SCDY (Rosenbaum *et al.*, 2020).

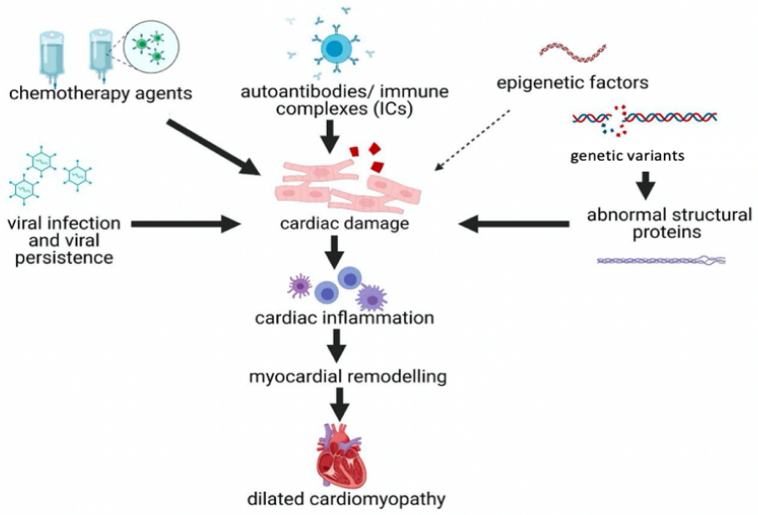

Figure 3 The causes of DCM are classified as acquired, familial or an interplay between genetic and environmental factors ('mixed'). Causes of DCM include genetic variants that effect structural proteins, viral infections, autoantibodies and ICs and toxic damage caused by chemotherapy treatments (Jain *et al.*, 2021).

Unlike most Mendelian disorders, genetic associations in FDCM have variable disease penetrance and clinical presentations (Seferović *et al.*, 2019). Sporadic manifestations of DCM may be the result of several, low penetrance alleles within the general public (Jain *et al.*, 2021). Genes implicated in the pathogenesis of FDCM are mainly involved in coding for proteins of the sarcomere, cytoskeleton, nuclear envelope, sarcolemma, cardiac ion channels, and/or intercellular junction molecules (Seferović *et al.*, 2019). Genetic variants are mainly inherited in an autosomal dominant fashion, but other patterns of inheritance have also been associated with FDCM, such as autosomal recessive, X-linked, and mitochondrial (Jain *et al.*, 2021).

The sarcomere structural protein titin, encoded by the *TTN* gene, is the largest gene found in the cardiac muscle tissues and is the most prevalent gene associated with FDCM (Shaboodien *et al.*, 2020). Variants in the *TTN* gene account for 25% of FDCM cases and 12% to 18% of sporadic DCM cases, however, genetic variants in the *TTN* gene are not usually linked to cardiac conduction defects (Rosenbaum *et al.*, 2020).

Variations in the Phospholamban (*PLN)* gene, which encodes the transmembrane protein in the sarcoplasmic reticulum (SR) - Phospholamban, have also been implicated in the pathogenesis of FDCM (Burke *et al.*, 2016). A specific founder variant (R14del) has been reported in both the Netherlands and Germany, resulting in a higher prevalence of FDCM in those populations (McNally & Mestroni, 2017).

Significant interest in the use of genetic markers in determining the projection of DCM as well as risk stratification is hindered by the fact that genetic testing in FDCM produces a relatively low diagnostic yield (30% to 35%) (Seferović *et al.*, 2019). This may be due to the variable aspects of the disease. However, one significant exception exists. The Lamin A/C nuclear envelope protein is encoded by the *LMNA* gene. Variants in the *LMNA* gene commonly result in both DCM and conduction system disease with the risk of SCD increasing by up to 46% in carriers (Rosenbaum *et al.*, 2020). Pathogenic variations in the *LMNA* gene are highly predictable for lethal arrhythmias and SCD (Burke *et al.*, 2016).

1.4 The *LMNA* gene

The major mammalian lamin proteins include A-type lamins and B-type lamins (Tatli & Medalia, 2018). B-type lamins (lamin B1 and B2) are encoded by *LMNB1* and *LMNB2* genes, respectively, and are expressed in all types of cells including stem cells and neurons (Captur *et al.*, 2018). Pathogenic variants in the *LMNB* genes are considered extremely rare and are not involved in the pathogenesis of cardiac diseases (Kang *et al.*, 2018). A-type lamins (lamin A and lamin C) are found, only, in completely differentiated cells and, unlike B-type lamins, are not expressed in stem cells nor cells of the central nervous system (Rankin & Ellard, 2006). A-type lamins are encoded by the *LMNA* gene.

The *LMNA* gene is located on the long arm of chromosome 1 (1q21.2-1q21.3), it is 24 kilobases (kb) in size and is made up of 12 exons (Genschel & Schmidt, 2000). Exon 1 to exon 10 is conserved between lamin A and lamin C proteins (lamin A/C proteins), with lamin C being generated from exon 10, which is transcribed by alternative splicing and translated into just six amino acids (figure 4) (Kang *et al.*, 2018). Exons 11 and 12 are exclusive to lamin A and exon 12 contains the sequence that codes for the carboxy-terminal CaaX (C, cysteine; a, aliphatic residue; X, any residue) box of prelamin A (Genschel & Schmidt, 2000). Prelamin A is matured into lamin A after integration into the nuclear lamina structure. The protease gene *ZMPSTE24* is responsible for lamin A maturation and accurate processing of prelamin A into lamin A is crucial for proper cell function and stability (Kang *et al.*, 2018).

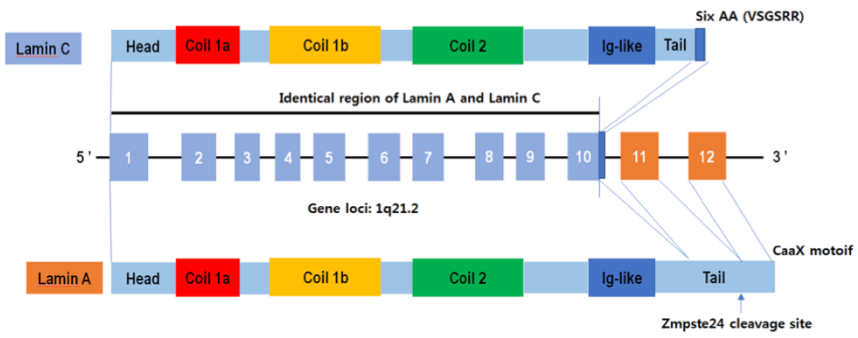

Figure 4 The *LMNA* gene is composed of 12 exons and two proteins, lamin A and lamin C. Exon 1 to exon 10 are identical between lamin A and lamin C, with lamin C being generated

from exon 10 which is transcribed by alternative splicing and translated into just six amino acids. Exons 11 and 12 are exclusive to lamin A and exon 12 contains the sequence that codes for the carboxy-terminal CaaX (C, cysteine; a, aliphatic residue; X, any residue) box of prelamin A. Prelamin A is processed by the ZMPSTE24 protease into mature lamin A (Kang *et al.*, 2018).

Lamin A/C are classified as IF proteins and form part of the nuclear envelope and cytoskeleton (Rankin & Ellard, 2006). All lamins, along with their binding partners-nuclear pore complexes (NPCs), form the nuclear lamina, a multimeric structure that is associated with the nucleoplasmic surface of the inner nuclear membrane (INM) (Genschel & Schmidt, 2000). The formation and structure of the nuclear lamina are shown in figure 5 below (de Leeuw *et al.*, 2018).

Lamin A/C filament structure is composed of an N-terminal head, a coiled-coil central rod domain - containing the unique nuclear localisation signal (NLS) and immunoglobulin (Ig) - fold domain- plus a CaaX motif at the C-terminal tail (de Leeuw *et al.*, 2018).

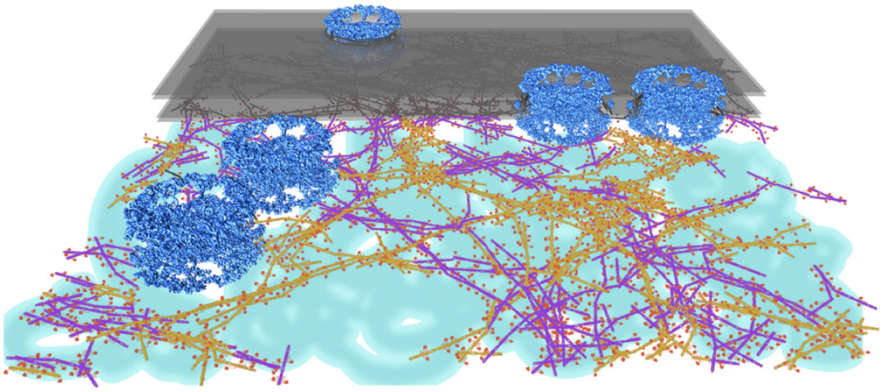

Figure 5 A-type lamins (gold), B-type lamins (purple), and NPCs (blue) form a meshwork structure below the INM, known as the nuclear lamina (de Leeuw *et al.*, 2018).

Structural analysis of the nuclear lamina shows that lamin A/C IF proteins form homodimers, which aggregate into head-to-tail polymers. Two polymers then interact, laterally, and form lamin protofilaments, which are 3.5 nanometres (nm) thick and have a specific beaded appearance due to the Ig folds found every 20 nm (figure 6a) (Tatli & Medalia, 2018). Lamin protofilaments further arrange, in a half-staggered fashion,

and form dense filamentous bundles that make up the nuclear lamina meshwork structure (figure 6b) (Captur *et al.*, 2018; de Leeuw *et al.*, 2018). The nuclear lamina aids in the structural support of the nucleus and protection of the chromatin, however, lamin A/C plays important roles in other processes such as chromatin organisation, deoxyribonucleic acid (DNA) repair, gene expression, and signal transduction (Captur *et al.*, 2018; de Leeuw *et al.*, 2018).

More than 600 point variants of the *LMNA* gene have been documented and are known to cause a spectrum of diseases in certain body tissues (Tatli & Medalia, 2018). Disease phenotypes caused by *LMNA* pathogenic variants are collectively termed laminopathies.

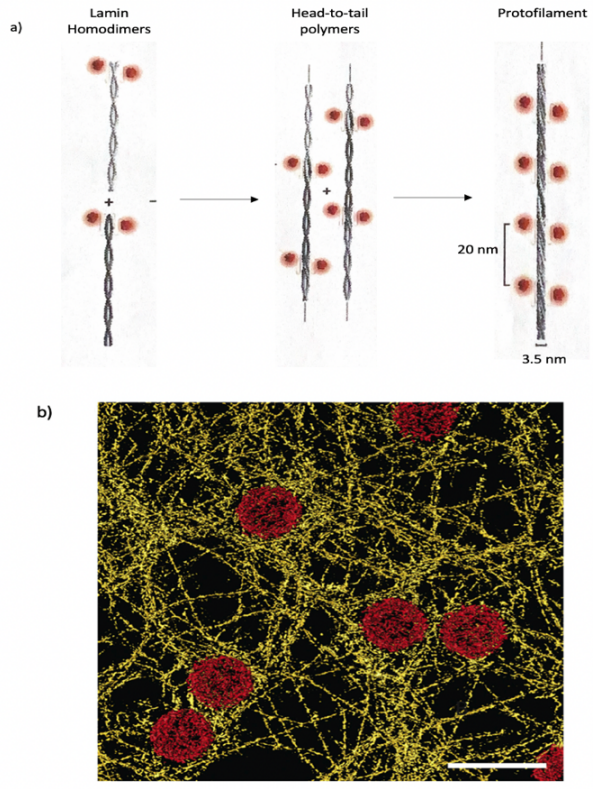

Figure 6(a) Lamin A/C IF proteins form homodimers, which aggregate into head-to-tail polymers. Two polymers then interact laterally and form lamin protofilaments which are 3.5 nm thick and have a specific beaded appearance due to the Ig folds found every 20 nm. **(b)** Lamin protofilaments further arrange in a half-staggered fashion and form dense filamentous bundles that make up the nuclear lamina's meshwork structure (seen in gold). The NPCs (shown in red) act as binding partners (de Leeuw *et al.*, 2018; Tatli & Medalia, 2018).

1.5 Laminopathies

A particularly intriguing characteristic of the *LMNA* gene variations is their ability to result in a diverse number of disease phenotypes (Rankin & Ellard, 2006). Most of the pathogenic *LMNA* variants or sequence-level alterations are missense variants but non-sense as well as intragenic deletions and duplications have also been implicated (Captur *et al.*, 2018).

Two hypothetic models have been suggested in an attempt to explain laminopathy phenotypes. The first, known as the 'structural-mechanical model' is based on the intense changes seen in the nuclear morphology – which may be attributed to the interruption of the filament formation (Tatli & Medalia, 2018). The disruption of the nuclear architecture results in nuclear fragility, which has been reported in skeletal muscle fibres, fibroblasts, and lymphoblastoid cells of patients with skeletal and cardiac laminopathies (Rankin & Ellard, 2006). The second hypothetic model, known as the 'gene expression model', suggests that genetic variants do not affect the physical structure of lamin A/C proteins, but instead negatively alter cellular signalling pathways and gene expression (Tatli & Medalia, 2018). This may result in a hindered interaction between lamin A/C proteins, chromatin, or other nucleic proteins (Rankin & Ellard, 2006).

The clinical effect of the variant differs depending on the molecular consequence of the predicted amino acid change (Captur *et al.*, 2018). Many 'hotspot' variants can result in laminopathy diseases in adipose, skeletal, cardiac, and nerve tissues as well as in the premature aging of body tissues (Tatli & Medalia, 2018). Emery-Dreifuss muscular dystrophy (EDMD), limb-girdle muscular dystrophy (LGMD), familial partial lipodystrophy (FPLD) type 2, Hutchinson-Guilford progeria syndrome (HGPS), and FDCM are all laminopathy disease phenotypes (Kang *et al.*, 2018). Although previously considered as separate diseases, the co-occurrence of more than one laminopathy phenotype in a family is well described. For example, in patients with EDMD and LGMD, DCM with conduction system disease is commonly found (Rankin & Ellard, 2006). These patients are, too, at an increased risk for SCD.

The most frequent cardiac phenotype of *LMNA* variants is FDCM (De Backer *et al.*, 2010). Mouse models, used to study the pathogenesis of FDCM, show a hindered response to mechanical stress suspected of promoting premature cardiac cell death (Burke *et al.*, 2016). Cardiac laminopathy, also known as lamin A/C heart disease (LHD), is marked by lethal supraventricular arrhythmias and atrial fibrillation (AF), which may occur before any overt structural changes (Captur *et al.*, 2018). This is different from most DCM-associated AF, hence the possible diagnosis of FDCM in a structurally normal heart. Cardiac laminopathies are characterised as a malignant disease with high penetrance (those affected will likely be symptomatic), early ventricular arrhythmias, atrioventricular (AV) block, and a rapid progression to HF (Hammersley & Halliday, 2020).

1.6 The local relevance of familial dilated cardiomyopathy and the *LMNA* gene

In contrast to developed countries, the main causes of HF, in Africa, are non-ischemic, such as FDCM (Agbor *et al.*, 2018). Dilated cardiomyopathy is one of the major causes of HF, globally. In a cohort of 156,013 HF patients in the USA, DCM was reported as the underlying cause in 31% of cases (Seferović *et al.*, 2019). In a retrospective study of case presentations in Ethiopia, DCM was reported as one of the most prevalent CVDs, accounting for 20% of cases (Keates *et al.*, 2017). Information on the prevalence of FDCM-associated variants in the South African population is lacking, even though, in the Heart of Soweto study, 35% of HF cases were attributed to DCM (Sliwa *et al.*, 2008).

Molecular genetic testing aids in the confirmation of diagnosis, disease prognostics, risk stratifications, and treatment protocols (Lee & Ching, 2019). Cardiovascular investigations and genetic testing can lead to a specific diagnosis in 40% of patients (De Backer *et al.*, 2010).

Despite the relatively low diagnostic yield in genetic testing of other FDCM-associated genes, *LMNA* gene variants are an important exception as they are highly predictable for DCM, with progressive and severe HF, as well as violent arrhythmias resulting in

SCD (Burke *et al.*, 2016). After reviewing all available literature to date, no single gene studies focused exclusively on the *LMNA* gene variants as a cause of FDCM, HF, or SCD in the South African population. By analysing this candidate gene, we could potentially 'rule in' or 'rule out' *LMNA* pathogenic variants as the cause of the scourge of DCM and HF in SA.

Considering the strong tendency of *LMNA* pathogenic variants resulting in an SCD, a genetic analysis of the *LMNA* gene in South African SCD cases, provides an optimal opportunity. High-resolution melt (HRM), real-time polymerase chain reaction (PCR) provides a simple, semi-automated, and cost-effective technique for variation detection in DNA samples (Millat *et al.*, 2009). Coupled with Sanger sequencing, an affordable, simple-to-use sequencing tool, which can be easily be reproduced in the detection of novel and existing pathogenic variants. This study aimed to determine the prevalence of FDCM-associated, pathogenic variants in the *LMNA* gene in SCD cases within the South African population.

1.7 Aim

This study aims to identify genetic variants of the *LMNA* gene, in individuals of the South African population, who died suddenly (SUD) due to suspected SCD.

1.8 Objectives

- To design primers for the 12 exons of the *LMNA* gene using primer design software.
- To optimize amplification conditions for the 12 exons of the *LMNA* gene using specifically designed primers and HRM real-time PCR.
- To detect *LMNA* variants in cases and controls by HRM real-time PCR and sequencing.
- To identify *LMNA* gene sequence variants by comparing case, control samples and a reference *LMNA* sequence downloaded from NCBI.
- To determine the type of variations (benign, unknown significance or pathogenic) found in the *LMNA* gene in a SUD cohort of the South African population, by searching biological databases, published data and using predictive software.

Chapter 2: Material and Methods

2.1 Study design

The study design was an observational, retrospective, case-control study. Genomic DNA was extracted from both case and control samples. The extracted DNA was used to amplify all exons of the *LMNA* gene. During sequencing analysis, case samples were compared to the control samples, in an attempt to identify any potential genetic variants. Variants, that were detected during sequencing analysis, were compared to previously known variants, which were listed on appropriate scientific databases (National Centre for Biotechnology Information (NCBI) or stated in previous literature.

2.1.1 Study setting

This study was conducted within the Department of Chemical Pathology, Faculty of Health Sciences at the University of Pretoria. This study was done in collaboration with the Department of Forensic Medicine, Faculty of Health Sciences at the University of Pretoria.

The case samples were collected during autopsy at the Pretoria Medico-Legal Laboratory (MLL). These samples were stored at -80 ºC within the Department of Chemical Pathology. Control sample collection was conducted at the Faculty of Health Sciences at the University of Pretoria. The control samples were, too, stored at the Department of Chemical Pathology.

2.1.2 Ethical considerations

Ethical approval, for this study, was granted by the Faculty of Health Science's Research Ethics Committee of the University of Pretoria, on the 26th of August 2021. The ethics reference number assigned to this study was 373/2021 and renewed on the 12th of August 2022 (Appendix A).

2.1.3 Access to case file information and storage

Permission from the manager of the Pretoria MLL was obtained, prior to commencement of this study, as part of the umbrella study. This permission granted access to case file information of the case samples that were used in this study, which were stored in the archival vaults at the Pretoria MLL.

All data sheets generated in this study as well as collected blood samples were stored at the Department of Forensic Medicine and at the Department of Chemical Pathology at the University of Pretoria.

2.1.4 Confidentiality

To ensure confidentiality of study participants, a study reference number was allocated to each case file. These reference numbers also ensured that the same case sample was not used more than once, during analysis, and to account and record the data obtained during this study. No personal information of participants was used on any data sheets, nor will they be used in this publication or any future publications that may be generated by the results obtained from this study.

2.1.5 South African regulation regarding retention and use of tissue samples obtained during a medico-legal post-mortem investigation

Existing regulations guide the retention and use of tissue and blood samples obtained at medico-legal post-mortem investigations conducted in SA (Toit-Prinsloo & Saayman, 2012). Section 3, subsection 2 of the Inquests Act 58 of 1959, authorises the retention of any internal organ or any part or any of the contents of the body, or any substance, by the district surgeon or any other medical practitioner, if he/she deems it necessary **for the purpose of ascertaining with greater certainty the cause of death.** Section 3, subsection 3 of the Inquests Act 58 of 1959, stipulates that “for the purpose of any examination mentioned in subsection 2, any part or internal organ or any of the contents of a body may be removed therefrom to any place”.

Similar regulations in accordance with the above-mentioned legislation are further substantiated by legislation stipulated in the National Health Act 61 of 2003. The retention and use of post-mortem blood samples in this study (only obtained from cases that firmly meets the set-out inclusion criteria) was lawfully and ethically justified as this study was conducted with the aim, as prescribed by the Inquests Act, to more accurately determine the cause of death- specifically attempting to identify a genetic variant as a possible cause of death.

2.2 Control samples

Control samples were collected from volunteers who provided written consent to partake in this study.

2.3 Population and sampling

The sample population was selected, according to the following criteria.

2.3.1 Inclusion criteria

The cases included in this study were of individuals who were referred to the Pretoria MLL as a possible SUD. The selected cases were of those whose cause of death remained unknown after a full and comprehensive medico-legal, post-mortem investigation. The autopsy investigation of these cases included toxicology, virology, and histopathological testing, all of which yielded no explanation for the sudden and unexpected death. The manner of death of these individuals was deemed natural deaths as there were no signs of trauma or accidental death. Included cases were those where the cause of death was suspected to be due to cardiac pathologies or SCD.

These individuals had no previous medical history, that could have led to their demise, nor any, potentially lethal, co-morbidities. These individuals included young children, aged between birth and one year (sudden unexpected death in infancy (SUDI) cohort) and young individuals aged between one and 45 years old (SUDY cohort). Case

samples were collected over a period of three years and the total n-number of case samples collected was 66 samples.

2.3.2 Exclusion criteria

Cases excluded from this study included cases where a cause of death could be determined after a post-mortem investigation. Individuals whose deaths were considered SCD due to ischemic heart diseases, such as CAD, hypertension, or congenital heart disease, were also excluded. Other excluding factors included the age of the individual (older than 45 years old).

2.3.3 Case samples

Whole-blood samples were collected, during autopsy, of individuals who had died suddenly and unexpectedly. These deaths were suspected to be due to SCD. In total, 66 case samples were collected over a period of three years (November 2017- April 2020).

2.3.4 Control samples

Venous blood samples were collected from consenting volunteers. The volunteers consisted of individuals who were in apparent good health and who had no medical history of CVD.

A consent form was presented to each selected volunteer. The consent form provided background regarding this study and explained the contribution of the volunteer. Within the consent form, it was made known to each volunteer that there was a possibility of detecting a potentially lethal variant, as SCD is usually the first and only symptom of an underlying genetic cardiac disease. Volunteers were asked whether they would have liked to be notified if such a variant was detected so that they could seek professional advice via our recommended genetic counsellor, Dr Engela Honey. Volunteers were required to provide written consent to participate in this study.

One ethylenediaminetetraacetic acid (EDTA) tube (approximately 5 mL) of whole-blood was collected from each consenting volunteer. A total of nine control blood samples were collected and used in this study.

2.4 Research procedure

The focus of this study was to investigate potentially pathogenic variants of the human *LMNA* gene. To analyse this gene, various molecular methods were used, including PCR, primer design and synthesis, extraction of genomic DNA from whole-blood samples, optimisation of PCR conditions, HRM real-time PCR analysis, sequencing of selected PCR products, via automated Sanger sequencing, sequencing analysis and genetic variant analysis.

Twelve PCR primer pairs were designed to cover the 12 exons, including intron-exon boundaries, of the *LMNA* gene. The primer pair sequences were sourced from literature in which previous analysis of the *LMNA* gene was conducted (Millat *et al.*, 2009). Finalised primer pair sequences were sent to Inqaba Biotech (Pretoria, SA) for synthesis. Once the synthesized primer pairs were received, they were subjected to primer optimisation to obtain the optimal PCR conditions for HRM real-time PCR analysis.

Genomic DNA was extracted from 66 case samples and nine control samples. The 12 exons of the *LMNA* gene were amplified using HRM real-time PCR. After HRM results were obtained, samples were grouped according to their melting profiles. These representative samples were selected and sent for sequencing to Inqaba Biotech (Pretoria, SA).

Once the sequencing results were obtained, the results were visualised on the Ugene Bioinformatics Software from Unipro (Novosibirsk, Russia). Case and control sequencing results were compared in an attempt to examine sequences for the presence of genetic variants. All identified genetic variants were examined by comparing them to already established variants listed on well-known scientific

databases (NCBI) or stated in the literature. The research procedure followed in this study is shown in figure 7 below.

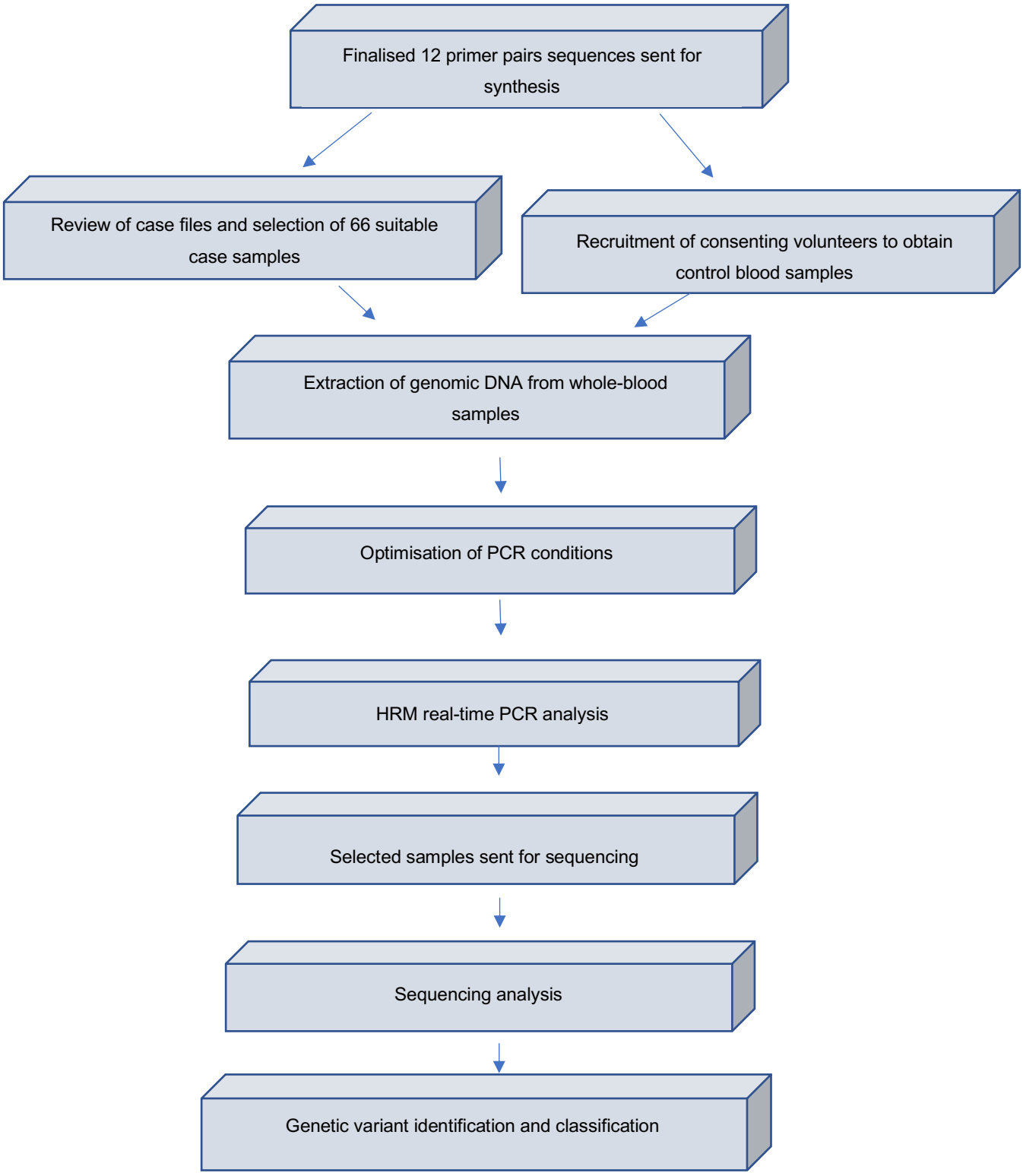

Figure 7 A flow diagram showing the research procedure used in this study

2.5 Materials

The equipment, kits, reagents, and services used, in this study, are listed as follows:

- Centrifugation processes- LABNET Prism™ R Refrigerated Microcentrifuge from Labnet (Edison, New Jersey (N.J.), USA)
- Determination of DNA concentration and quality- Nanodrop™ 2000/2000c spectrophotometer from ThermoFisher Scientific (Waltham, Massachusetts (Mass.), USA)
- PCR amplification- RotorGene®® Q multiplex HRM platform from Qiagen (Hilden, Germany)
- DNA extractions- QIAamp DNA Blood Mini Kit (50) from Qiagen (Hilden, Germany)
- HRM analysis -SENSIFAST® HRM kit from Bioline (London, United Kingdom (UK))
- Primer synthesis was done by Inqaba Biotec (Pretoria, SA)
- DNA sequencing was done in collaboration with Inqaba Biotec (Pretoria, SA)
- DNA sequencing analysis - Unipro Ugene Bioinformatics Software (Novosibirsk, Russia)

2.6 Primer synthesis

Primer pair sequences, which covered the 12 exons of the *LMNA* gene, were sourced from literature (Brown *et al.*, 2001; Millat *et al.*, 2009; Nishiuchi *et al.*, 2017). In total, 12 primer pairs were selected to amplify the *LMNA* gene. These primer pair sequences, and their corresponding fragment lengths are shown in table 1, below. The primer pair sequences were aligned to the RefSeq gene on the Unipro Ugene Bioinformatics Software (Novosibirsk, Russia) to ensure that binding occurred in the correct positions i.e., that the correct fragments were amplified. The specificity of each primer pair was determined using the basic local alignment search tool (BLAST) on

the NCBI website. Once the primer pair sequences were confirmed, they were sent to Inqaba Biotech (Pretoria, SA) for synthesis.

Table 1 The 12 primer pair sequences used to amplify the 12 exons of the *LMNA* gene

Exon	Primer name	Forward Sequence (5' to 3')	Reverse Sequence (5' to 3')	Fragment Length (in bp)	Primer pair obtained from:
1	1A	TCTCTGTCCTTCGACCCGAG	CCTCTCCACTCCCCGCCA	477	(Brown *et al.*, 2001)
2	2A	ACAGACTCCTTCTCTTAAATCTAC	GTAGAAGAGTGAGTGTACATGTG	264	(Brown *et al.*, 2001)
3	3A	TGTTCTGTGACCCCTTTTCC	AGCCCAAGTCTGTCATCACC	228	(Millat *et al.*, 2009)
4	4A	GGCCTCCCAGGAACTAATTCTG	CTCCCTGCCACCATCTGC	334	(Millat *et al.*, 2009)
5	5A	GCAGTGATGCCCAACTCAGG	ATCTCAGACCCGGCCTACGT	257	(Nishiuchi *et al.*, 2017)
6	6A	GCCAAGACTATGTTTAGAGCTTG	GTTGACCGGAACTGATCTGG	466	(Nishiuchi *et al.*, 2017)
7	7A	AGTGTCCTCTGGCCGGCAAC	GTCTCCCACCTGGTCCCACT	400	(Nishiuchi *et al.*, 2017)
8	8A	GAGGCCTCAATTGCAGGCAGGC	ACCCAAGGCCTCCCCAGAG	252	(Millat *et al.*, 2009)
9	9A	GGAGCGCTGGGGTAAGTGTC	CTCGTCCAGCAAGCAGCCAG	192	(Millat *et al.*, 2009)
10	10A	CTGACCCTTGGACCTGGTT	AGGGAGGAGAGAGAAGAAAGG	281	(Millat *et al.*, 2009)
11	11A	GTTGGGCCTGAGTGGTCAG	CACCTCGTCCTACCCCTCG	404	(Brown *et al.*, 2001)
12	12A	CTTGTCTGAGCCCCAGACTGGAG	TAAAGAGGAGGGAAGGAAAAGGGA	436	(Nishiuchi *et al.*, 2017)

Once synthesized, the primers were received in a lyophilized form and were prepared according to the instructions provided by Inqaba biotech (Pretoria, SA). This preparation process involved rehydrating the lyophilized primers into a solubilized solution. The primer solution was divided into four aliquots of a concentration of 100 pmol/μL each. The aliquots were used as stock solutions. Working solutions were prepared from the stock solutions. A volume of 10 μL of primer stock solution was diluted with 90 μL of distilled water to produce a working solution with a final concentration of 10 pmol/μL. The stock and working solutions were stored at -20 ºC, in separate containers to avoid contamination.

2.7 DNA extraction from whole-blood samples

Genomic DNA was extracted from whole-blood samples, collected from both cases and controls. The QIAamp DNA mini blood kit (50) from (Qiagen, Germany) was used for DNA extraction.

2.7.1 DNA extraction procedure

The protocol followed to extract genomic DNA was according to the instructions provided by the manufacturer- (Qiagen, Germany). The DNA extraction process is explained, in detail, in appendix B. The purified DNA solutions, were collected in 1.5 mL microcentrifuge tubes and were stored at -20 ºC, to be used at a later stage in the research procedure.

2.8 Determination of DNA concentration and purity

To ensure that the DNA extracted from the whole-blood samples, was suitable for PCR amplification and HRM analysis, the DNA concentration and the purity of the DNA were determined. The Nanodrop™ 2000/2000c spectrophotometer (ThermoFisher Scientific) was used to determine the concentration and purity of the extracted DNA solution. At commencement, the spectrophotometer was blanked when 2 μL of buffer AE was pipetted onto the pedestal of the spectrophotometer and the machine was set

to 'blank'. Thereafter, the buffer AE was cleaned off with laboratory-grade tissue paper and two μL of the extracted DNA solution was, then, pipetted onto the pedestal. The resulting DNA concentration and purity were observed on the light-emitting diode (LED) screen on the instrument. These results were noted and recorded in appendix D.

2.9 PCR optimisation

PCR optimisation was conducted to determine the optimal PCR conditions for each primer set of the 12 *LMNA* gene exons (set A). This was necessary to ensure successful amplification of the DNA target.

The PCR optimisation began with the preparation of a 'mastermix' solution. The composition of the mastermix solution included autoclaved PCR-grade H_2O, SENSIFAST® HRM kit (Bioline,UK) and control template DNA. The SENSIFAST® HRM kit (Bioline,UK) consisted of 3rd generation fluorescent dye EVAGREEN®, DNA polymerase and buffer solution. Each PCR optimisation reaction contained the same template DNA, obtained from a control blood sample. The composition of the 'mastermix' solution is shown in table 2. Each reaction tube contained different primer pair working solutions (10 μM), specifically selected to investigate their optimal PCR conditions. The exact composition of each reaction tube is shown in table 3 below. The PCR optimisation process involved dividing the prepared mastermix solution into 0.5 mL tubes and then adding 2 μL of both the forward and reverse primer solution, chosen for optimisation.

Table 2 Composition of the 'mastermix' solution used in the PCR optimisation process

Reagents	**Volume (μL)**
SENSIFAST® HRM kit	10
PCR-grade H_2O	10
DNA control template (18.251 μM)	2
Total Volume	22

Table 3 Composition of each reaction tube used in the PCR optimisation process

Reagents	**Volume (μL)**
SENSIFAST® HRM kit	10
PCR-grade H_2O	10
Selected forward primer solution (10 μM)	2
Selected reverse primer solution (10 μM)	2
DNA control template (18.251 μM)	2
Total Volume	26

The tubes were then loaded into the rotor of the RotorGene® Q multiplex HRM platform (Qiagen, Germany).

The initial PCR conditions were set as follows:

Hot Start Denaturation: 95 ºC for 10 minutes

Denaturation: 95 ºC for 10 seconds

Initial Primer annealing: determined by subtracting 5 ºC from the unique melting temperature (Tm) of each primer pair

Extension: 72 ºC for 10 seconds

40 cycles

HRM cycle: 75 ºC to 95 ºC rising 0.1 ºC every two seconds

Once the run was completed, the PCR melt curve was analysed to confirm the accurate amplification of the DNA target. If any non-specific binding took place or if no amplification was detected then the annealing temperature was increased by 1 ºC to 2 ºC. Other conditions that were manipulated included the annealing time and the extension time. Once the optimal PCR amplification conditions were obtained, the primers were then ready to be used in HRM analysis.

2.10 Agarose gel electrophoresis

Agarose gel electrophoresis was used to visualise the target PCR product and confirm successful PCR amplification following every real-time PCR optimisation run. Although real-time PCR analysis is considered a sensitive tool for detecting DNA amplification, the intercalating agent present in the SENSIFAST® premix does not target a specific amplicon and rather binds to the amplified DNA. Hence, agarose gel electrophoresis was used to validate the successful amplification of the desired PCR product based on the correct band size (bp).

A 3% agarose gel was prepared by dissolving three 0.5 grams (g) Bioline agarose tablets (DNase/RNase free) in 150 mL 1 x Tris-acetate-EDTA (TAE) buffer (see Appendix C for composition). The TAE buffer with the agarose tablets were combined in a laboratory grade flask. The agarose tablets were dissolved within the TAE buffer completely before the flask was heated in the laboratory microwave for two to three minutes.

The flask, containing the dissolved gel solution, was cooled by holding the sealed flask under a cool stream of water. The flask was continuously stirred to ensure that the gel did not set within the flask. Once cooled to the touch, 6 μL of 10 mg/mL Ethidium Bromide (EtBr) stock solution from Sigma-Aldrich (St. Louis, Missouri (Mo.), USA) was added to the gel solution. The solution was mixed thoroughly until the EtBr was incorporated.

The gel solution was slowly poured into a gel-casting tray with a gel comb in place. The gel was left to set, until firm, for 30 minutes. After this, the gel comb was carefully removed from the set gel revealing the wells. The gel was then submerged into the electrode chamber, which had been filled with the same TAE buffer used to prepare the agarose gel. Thereafter, 5 μL of the 50 bp DNA Hyperladder (Bioline, UK) (figure 8), was pipetted into the first and last wells of the submerged gel. Following this, 3 μL of each PCR sample (from each of the 12 exons of the *LMNA* gene) were mixed, individually, with 2 μL of 5x sample loading buffer/dye on laboratory-grade parafilm

paper. Each sample-loading buffer mixture were then pipetted into their corresponding wells in the gel. An electric current of 100 volts (V) was run through the electrode chamber for one hour and 20 minutes. This ensured sufficient separation of the PCR products.

Once the time period had lapsed, the gel was removed from the electrode chamber and placed under a UV light. The gel was visualised using the Transilluminator UVITECH Firereader (Cambridge, UK). Optimised PCR conditions for each exon was confirmed by a single, clear band corresponding to the correct size band on the DNA hyperladder. If multiple bands were visable, it indicated that the PCR conditions for the particular exon required adjustments to improve the primer performance.

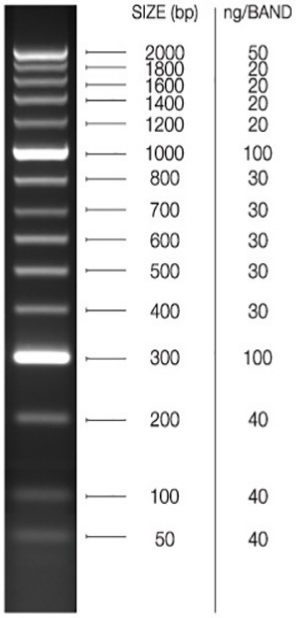

Figure 8 Bioline 50 bp (base pair) DNA hyperladder used in the agarose gel electrophosis processes described above. The ladder is read from first faint band (from the bottom), indicating a 50 bp band size. The first indicator band is shown by a bright band at 300 bp and the second indicator band is the bright band seen at 1000 bp. The final band in the DNA hyperladder is indicated by the uppermost, bright band at 2000 bp.

2.11 HRM real-time PCR analysis

Case samples and control samples were subjected to HRM real-time PCR analysis. The 12 exons of the *LMNA* gene were examined through the use of their respective primer pairs. The samples, along with the selected primers (corresponding to the exon being analysed) were run under the optimised conditions, obtained during the PCR optimisation process.

A mastermix solution was prepared in a 1.5 μL tube. The composition of the mastermix solution was, as shown in table 4, except the DNA sample was not included in the mastermix as different DNA samples were analysed during the same PCR run. The volume of the mastermix solution was altered depending on the number of reactions. Each reaction consisted of a duplicate pair of 0.1 μL PCR tubes, containing equal volumes of the mastermix solution (12 μL).

Table 4 The mastermix solution used in the HRM real-time PCR analysis process.

Reagent	**Volume (μL)**
SENSIFAST® HRM kit	10
PCR-grade H_2O	10
Forward Primer Solution (10 μM)	2
Reverse Primer Solution (10 μM)	2
Total reaction volume	24 (divided between two 0.1 mL tubes)

Thereafter, 2μL of a specific DNA sample was added to each corresponding duplicate tube to complete the reaction solution. The final volume in each 0.1 mL PCR tube was 14 μL.

High resolution melt analysis of case and control samples were performed in order to group samples according to their specific HRM melting curve patterns. After PCR amplification and HRM analysis, samples were grouped according to the melting profile obtained, for example, if sample 1 and sample 2 showed the same melting profile, they would be grouped together. A representative sample, from each group,

was then selected and stored at -20 ºC. This process continued until all 66 case samples and nine control samples had been analysed and grouped accordingly.

The final step of this process involved subjecting the representative samples to HRM analysis once more. The representative samples were grouped, again, according to their melting profiles. This additional step was done to reduce the sample pool and to obtain the most accurate representative samples for sequencing analysis. This step also aided in reducing the waste of PCR reagents and reduction of sequencing costs. Once the representative samples were finalised, they were sent for sequencing.

2.12 Sanger sequencing

Samples were sent to Inqaba Biotech (Pretoria, SA) for sequencing via automated Sanger sequencing. Both the forward and reverse direction for each sample were sequenced to ensure the validity of any identified variants. Sequencing results were received in the form of chromatograph files and visualised using the Unipro Ugene Bioinformatics Software (Novosibirsk, Russia).

2.13 Sequence variant analysis

Sanger sequencing results, in the form of chromatographs, were received from Inqaba Biotech (Pretoria,SA) via e-mail. Each chromatograph was analysed using the Unipro Ugene Bioinformatics Software (Novosibirsk, Russia). Chromatographs of each representative case and control samples were analysed individually.

The initial step was to align each forward and reverse sequence (obtained from the chromatograph files) to the *LMNA* reference sequence (NG_008692.2), obtained from the NCBI database. This was done in order to identify any variations in the chromatograph sequence. Each ambiguous character was examined to determine if they were possible sequence variants or if they were simply miscalled bases. Each possible variant was noted by recording its sequence reference position.

Following this, all chromatographs with identified possible variants, were aligned to the coding DNA (cDNA) sequence of the *LMNA* gene (NM_170707.4). The reference position of the variant on the cDNA sequence was noted. This aided in the determination of the position of the variant in the *LMNA* amino acid sequence.

Thereafter, the chromatograph sequences were exported and translated into amino acid sequences via the Unipro Ugene Bioinformatics Software (Novosibirsk, Russia). These sequences were then aligned to the *LMNA* amino acid sequence (NP_733821). Any and all changes in the amino acid sequences were recorded as identified sequence variants. The next step was to analyse the identified variants. Each variant was searched for via various international variation databases such as ClinVar, NCBI, dbVAR, dbSNV and ClinVar Miner, as well as all previously published articles on *LMNA* gene variants. This was done in order to 'sort' the identified variants into 'known' variants or 'unknown'/ 'novel' variants.

Chapter 3: Results

3.1 DNA extraction and quality

Genomic DNA was extracted from the 66 case samples and nine control samples that were selected for this study. Initially, the ReliaPrep Blood gDNA Miniprep System extraction kit (Promega, Wisconsin) was used to perform the DNA extractions. However, it was noted that the resulting DNA concentrations were insufficient for use in downstream PCR applications. Instead of wasting limited whole blood samples by continuously attempting to re-extract DNA, in hopes of yielding a better concentration, the decision was made to use the QIAamp DNA Blood Mini kit (50) (Qiagen, Germany)- as stated in the material and methods.

The concentrations of the DNA extracted from the 66 case samples and nine control samples, ranged from 11,473 µg/mL to 112,81 µg/mL. The purity ratio of absorbance (260 nm/ 280 nm) for all case and control samples, ranged from 1.717 to 2.903. The volumes of eluted DNA obtained from each DNA extraction were between 100 - 200 µL (according to the manufacturer's instructions). This volume of eluted DNA provided enough template DNA for the initial PCR amplification of the 66 case samples and nine control samples. However, as the study progressed, there was a need to obtain more template DNA for analysis so certain samples were subjected to a second DNA extraction to obtain the sufficient DNA template needed to complete PCR amplification and HRM analysis. Further information detailing the results obtained during the subsequent DNA extraction process (individual concentrations and purity ratios for all case and control samples) can be seen in Appendix D.

3.2 Primer design

The initial 12 primer sets (set A) were documented in Chapter 2: Material and methods of this study (see section 2.6 Primer synthesis). Following the PCR optimisation process, primers 1, 5, 6, 7, 10, 11, and 12 were redesigned using the Primer3web V

4.1.0 software. The redesigned primers and corresponding fragment lengths can be seen in table 5 (set B), below.

Table 5 Redesigned primer pairs used to amplify exons 1, 5, 6, 7, 10, 11 and 12 of the *LMNA* gene.

Exon	Primer pair	Forward Sequence (5' to 3')	Reverse Sequence (5' to 3')	Fragment Length (bp)
1	1B	CGAGTCTGAAGAGGTGGTCA	GCTCCTTAAACTCCTCACGC	155
5	5B	GGCAGTCTGCTGAGAGGAAC	GCTTCTGGAGCTGGCTGAG	111
6	6B	CTGCTGGCGGAAAAGGAG	CTCGCCCTCCAAGAGCTT	141
7	7B	TCACTCATCCCAGACACAGG	TCATTGGACTTGTTGCGCAG	168
10	10B	AGTGACTGTGGTTGAGGACG	TTTTGGCACGGGGAGGCT	152
11	11B	ACCCCGCTGAGTACAACC	GAGGTAGGAGCGGGTGAC	218
12	12B	TTCCACTACACCTGGCTGAG	CTTCCACCTCCCACCTCATT	157

The PCR process was repeated on the new primer sets (set B), shown above. Primer set 12 was redesigned, using the Primer3web V 4.1.0 software. The redesigned primer and the corresponding fragment length can be seen in table 6 and labeled set C.

Table 6 Redesigned primer pair 12 used to amplify exon 12 of the *LMNA* gene.

Exon	Primer pair	Forward Sequence (5' to 3')	Reverse Sequence (5' to 3')	Fragment Length (bp)
12	12C	AATGAGGTGGGAGGTGGAAG	CTCCCCTTTCCAGTGACCTC	151

3.3 Optimisation of PCR conditions for the 12 primer pairs of the *LMNA* gene

The standard, optimised reaction mixture used during the primer optimisation process is shown in table 7. Each primer pair reaction was prepared according to the reaction mixture below, however, certain primers were optimised at different concentrations.

Table 7 Optimised reaction mixture used for HRM with pre-amplification of the 12-primer pairs.

Reagents	Volume (µL)
SENSIFAST® HRM kit	10
PCR-grade H_2O	10
Forward Primer Solution (Variable concentration*)	2
Reverse Primer Solution (Variable concentration*)	2
DNA (concentration:11,473 µg/mL to 112,81 µg/mL) from case/control sample	4
Total Volume	28

The specific concentration for each primer pair is shown in **table 8.*

Table 8 Optimised primer concentrations used for HRM with pre-amplification of the 12-primer pairs.

Primer pair	Primer concentration (µM)
Exon 1	10

Primer pair	Primer concentration (μM)
Exon 2	10
Exon 3	5
Exon 4	10
Exon 5	10
Exon 6	10
Exon 7	10
Exon 8	10
Exon 9	10
Exon 10	10
Exon 11	5
Exon 12	10

The PCR reaction settings were similar for all primer pairs (table 9) with the primer annealing temperatures and times being the only conditions that differ among the 12 primer pairs.

Table 9 PCR reaction settings used for PCR optimisation of the 12 primer pairs.

	Temp	Time	# of Cycles
Hot Start Denaturation:	95 ºC	10 minutes	1
Denaturation:	95 ºC	10 seconds	40
Primer annealing:	Variable temp*	Variable times*	
Extension:	72 ºC	10 seconds	
HRM cycle	75 ºC to 95 ºC	rising 0.1 ºC every two seconds	1

The primer annealing settings, specific to each primer pair, are shown in **table 10 below.*

Table 10 Optimised primer annealing settings used for PCR optimisation of the 12 primer pairs.

Primer Pair	Annealing temp (ºC)	Annealing time (seconds)
Exon 1	67	10
Exon 2	60	10
Exon 3	66	8
Exon 4	60	10
Exon 5	68	10
Exon 6	67	8
Exon 7	66	10
Exon 8	67	10
Exon 9	67	10
Exon 10	69	10
Exon 11	68	10
Exon12	68	10

3.3.1 Primer pair 1

By using these optimised PCR conditions, amplification of the target DNA template was achieved as shown in figure 9 below.

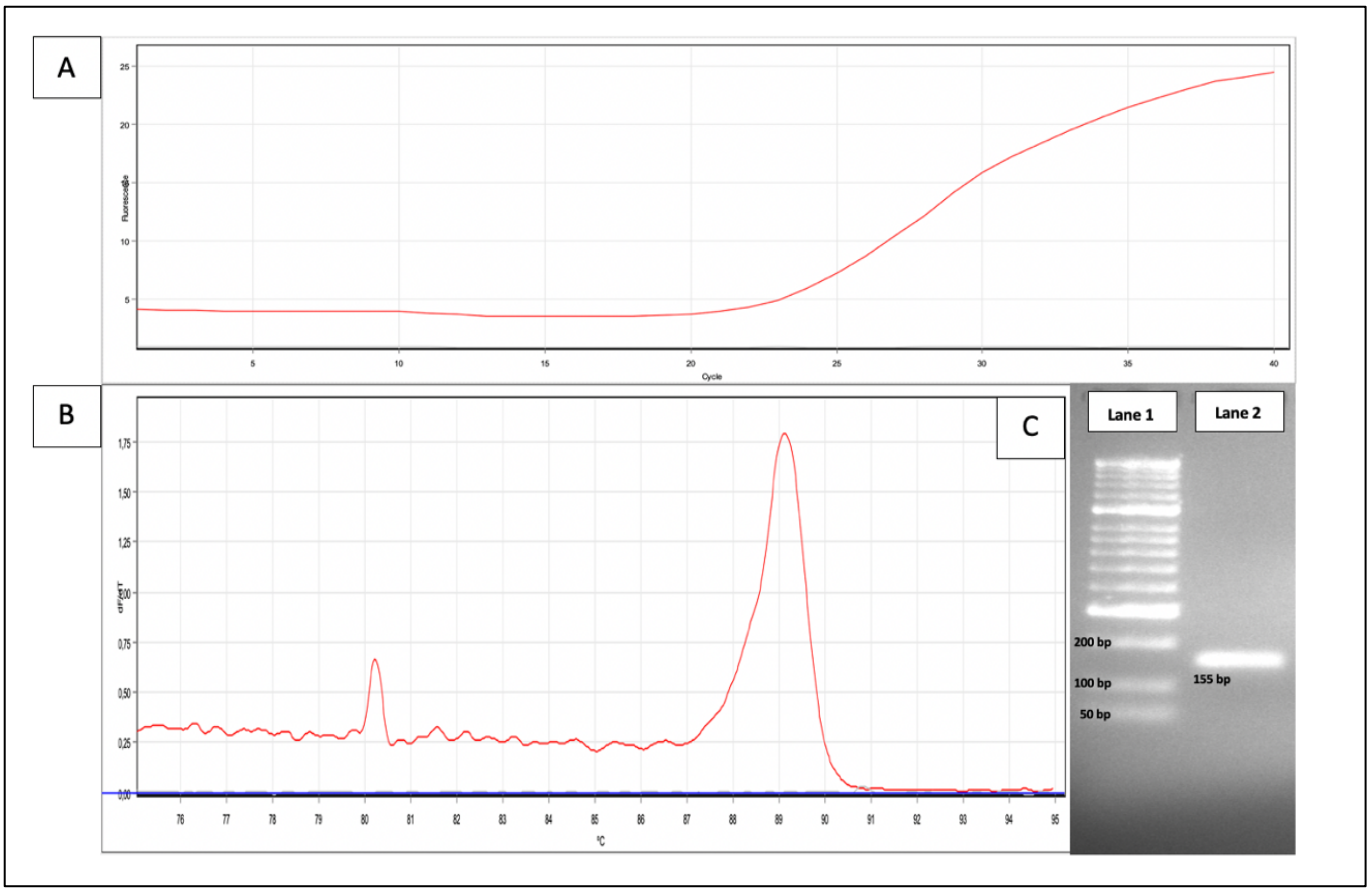

Figure 9: Graphs obtained following HRM with pre-amplification of exon 1.

A) The graphical output of the real-time PCR analysis shows amplification on the HRM channel. Fluorescence was detected at approximately 24 cycles as indicated by an increase in the slope of the red line. The slope reaches a plateau at approximately 40 cycles. The no template control (NTC) line is not seen on the graph as no fluorescence was detected.

B) The derivate of fluorescence over temperature versus temperature (dF/dT vs Temp) curve or the fluorescence melt curve shows a single, tall peak (red line) at approximately 89,5 ºC. A small, obscure peak is detected at approximately 80,2 ºC. No peak is detected in the NTC (purple line) which eliminates the possible occurrence of reagent contamination.

C) The 2% agarose gel shows a single, bright band at the correct product size of 155 bp (lane 2) when compared to the 50 bp molecular weight marker seen in lane 1.

3.3.2 Primer pair 2

By using the optimised PCR conditions, amplification of the target DNA template was achieved for exon 2, as shown in figure 10 below.

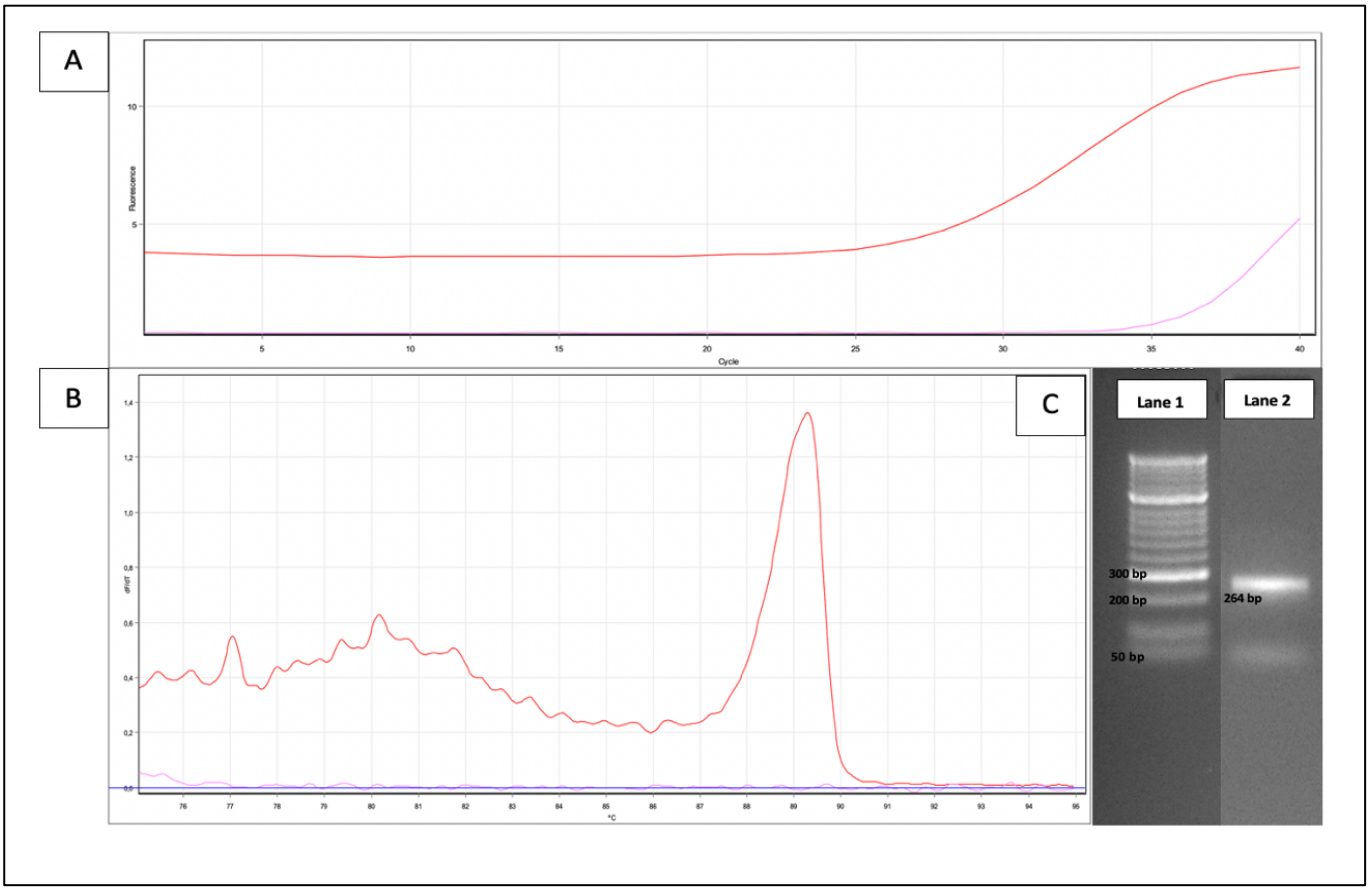

Figure 10 Graphs obtained following HRM with pre-amplification of exon 2.

A) The graphical output of the real-time PCR analysis shows amplification on the HRM channel. Fluorescence was detected at approximately 29 cycles as indicated by an increase in the slope of the red line. The slope reaches a plateau at approximately 40 cycles. The NTC is indicated by the pink line on the graph. The NTC shows a slight increase in fluorescence, which was detected at approximately 34 cycles.

B) The dF/dT vs Temp. curve or the fluorescence melt curve shows a single, tall peak (red line) at 89,5 ºC. This peak indicates the desired PCR product. Random amplification is seen to the left of the main peak. No peak is detected in the NTC (pink line) which eliminates the possible occurrence of reagent contamination.

C) The 2% agarose gel shows a single, bright band at the correct product size of 264 bp (lane 2). Below the main band, there is a very faint second band seen at approximately 50 bp when compared to the 50 bp molecular weight marker seen in lane 1.

3.3.3 Primer pair 3

By using the optimised PCR conditions, amplification of the target DNA template was achieved for exon 3, as shown in figure 11 below.

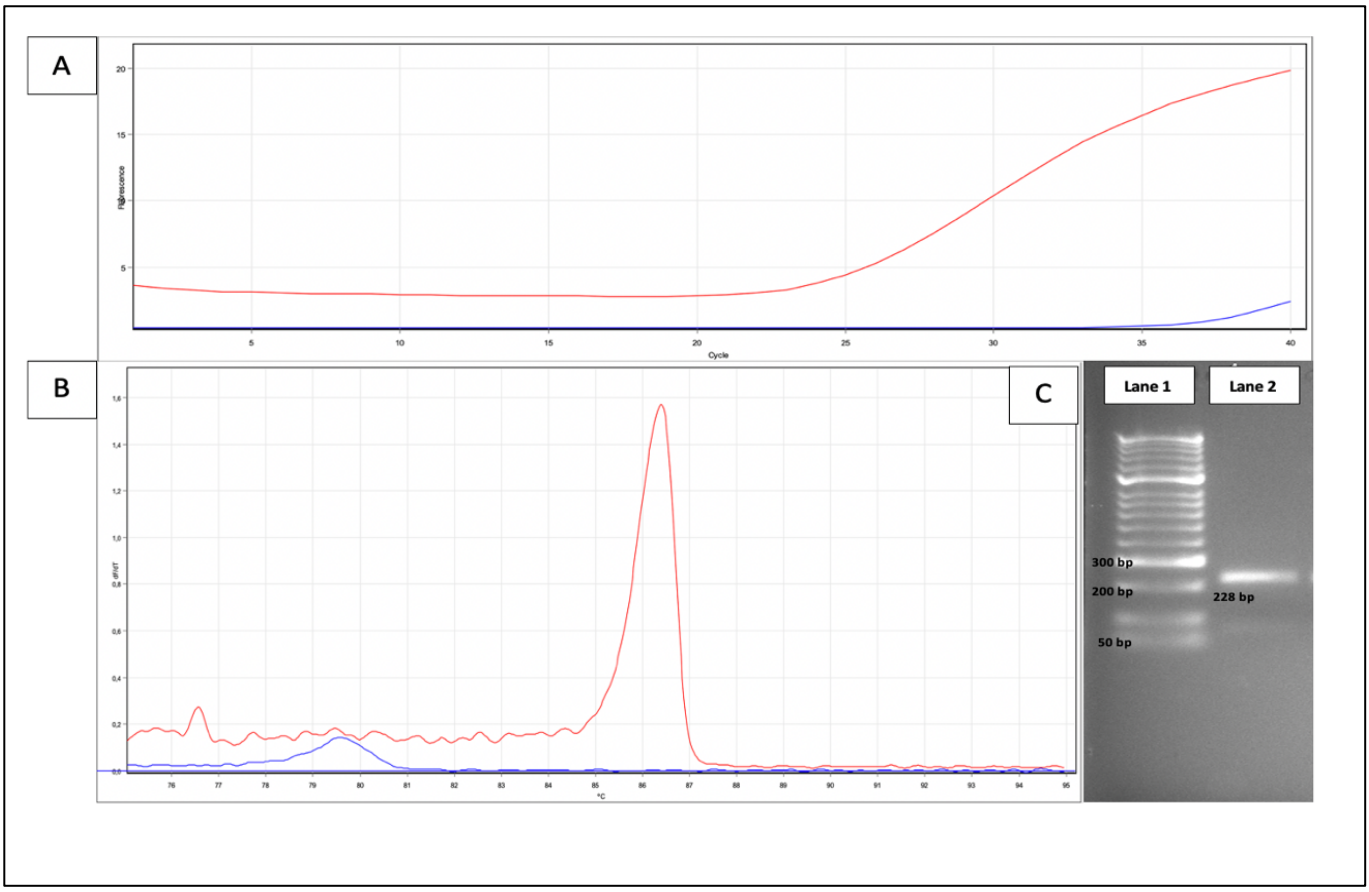

Figure 11 Graphs obtained following HRM with pre-amplification of exon 3.

A) The graphical output of the real-time PCR analysis shows amplification on the HRM channel. Fluorescence was detected at approximately 24 cycles, indicated by an increase in the slope of the red line. The slope reaches a plateau at around 40 cycles. The NTC is indicated by the blue line on the graph. The NTC shows a slight increase in fluorescence, which was detected at approximately 35 cycles.

B) The dF/dT vs Temp. curve or the fluorescence melt curve shows a single, tall peak (red line) at 86,5 ºC. This peak indicates the desired PCR product. There is a very small peak seen to the left of the main peak at approximately 76,5 ºC. No significant peak is detected in the NTC (blue line) which eliminates the possible occurrence of reagent contamination.

C) The 2% agarose gel shows a single bright band at the correct product size of 228 bp (lane 2). Below the main band, a very faint second band is seen between 50 bp and 100 bp when compared to the molecular weight marker seen in lane 1.

3.3.4 Primer pair 4

By using the optimized PCR conditions, amplification of the target DNA template was achieved for exon 4, as shown in figure 12 below.

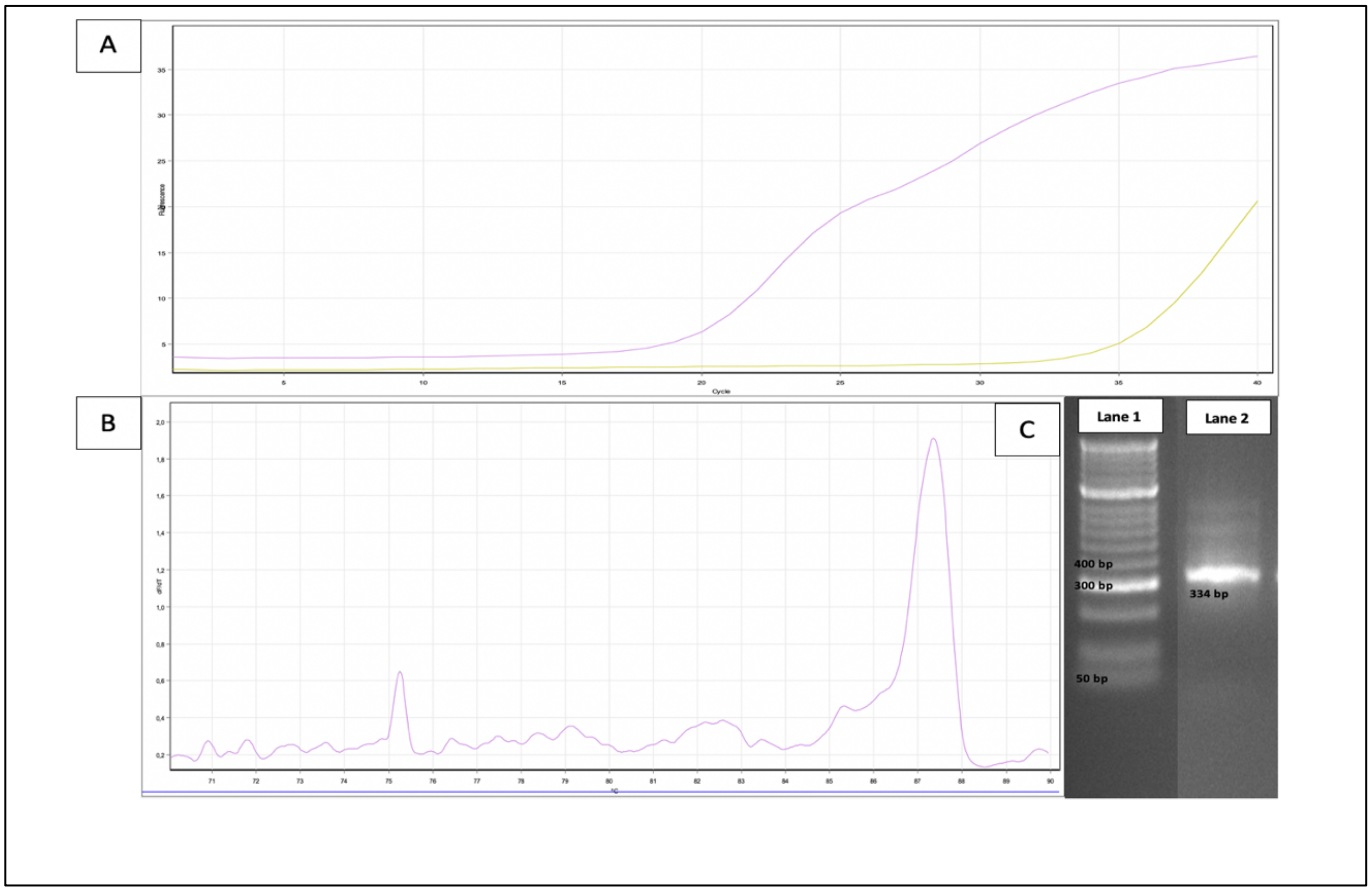

Figure 12 Graphs obtained following HRM with pre-amplification of exon 4.

A) The graphical output of the real-time PCR analysis shows amplification on the HRM channel. Fluorescence was detected at approximately 19 cycles, indicated by an increase in the slope of the pink line. The slope reaches a plateau at approximately 40 cycles. The NTC is indicated by the yellow line on the graph. The NTC shows a slight increase in fluorescence, detected at 34 cycles.

B) The dF/dT vs Temp. curve or the fluorescence melt curve shows a single, tall peak (pink line) at approximately 87,5 ºC. This peak indicates the desired PCR product. There is a very small peak seen to the left of the main peak at approximately 75,3 ºC and random amplification is seen preceding the main peak. No significant peak is detected in the NTC (yellow line), which eliminates the possible occurrence of reagent contamination.

C) The 2% agarose gel shows a single, bright band at the correct product size of 334 bp (lane 2). Above the main band, a faint smear can be seen.

3.3.5 Primer pair 5

By using the optimized PCR conditions, amplification of the target DNA template was achieved for exon 5, as shown in figure 13 below.

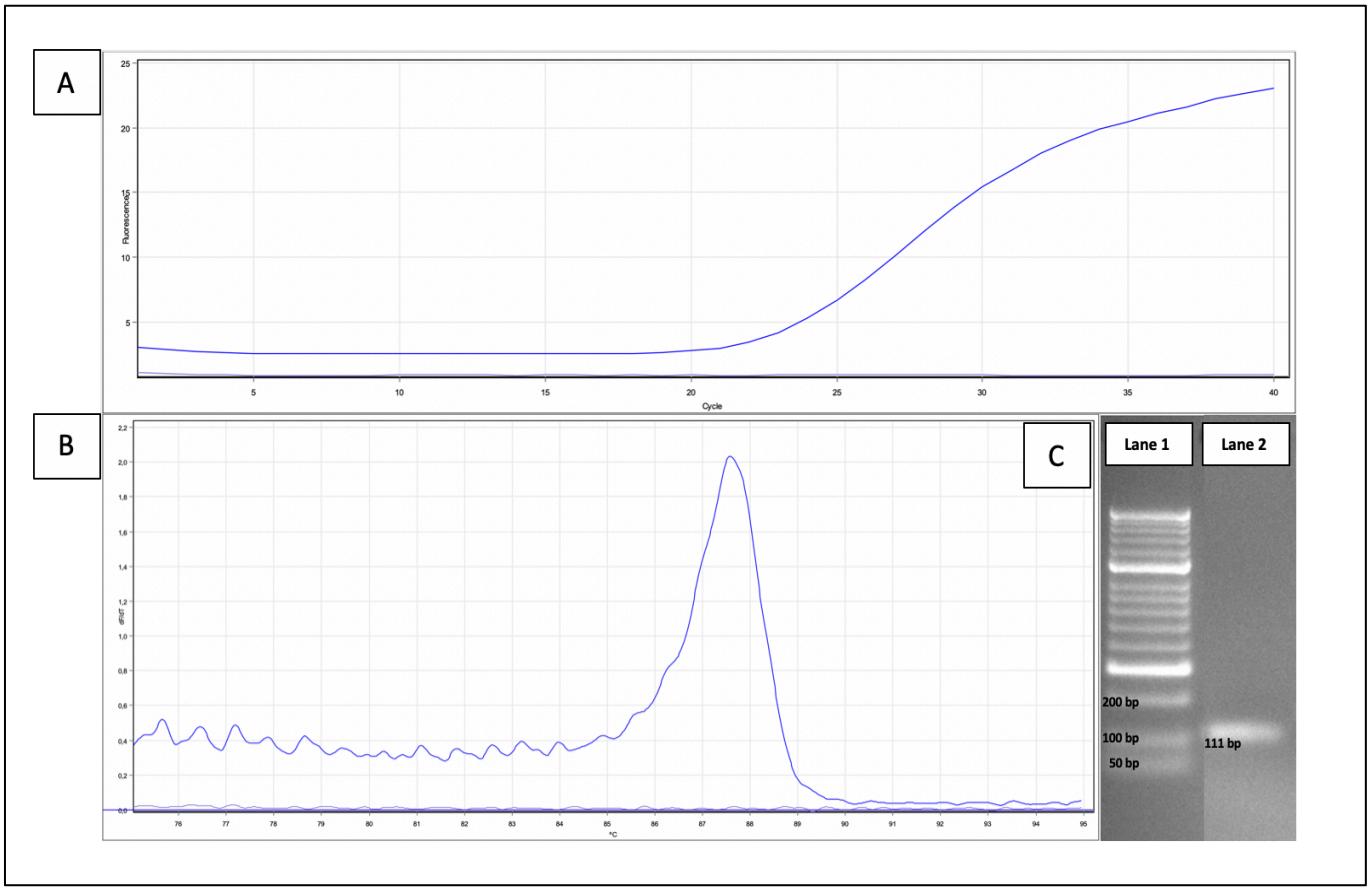

Figure 13 Graphs obtained following HRM with pre-amplification of exon 5.

A) The graphical output of the real-time PCR analysis shows amplification on the HRM channel. Fluorescence was detected at approximately 22 cycles, indicated by an increase in the slope of the blue line. The slope reaches a plateau at around 40 cycles. The NTC is indicated by the flat, violet line shown on the graph.

B) The dF/dT vs Temp. curve or the fluorescence melt curve shows a single, tall peak (blue line) at approximately 87,5 ºC. This peak indicates the desired PCR product. There is random amplification seen preceding the main peak. No significant peak is detected in the NTC (violet line) which eliminates the possible occurrence of reagent contamination.

C) The 2% agarose gel shows a single bright band at the correct product size of 111 bp (lane 2) when compared to the molecular weight marker seen in lane 1.

3.3.6 Primer pair 6

By using the optimized PCR conditions, amplification of the target DNA template was achieved for exon 6, as shown in figure 14 below.

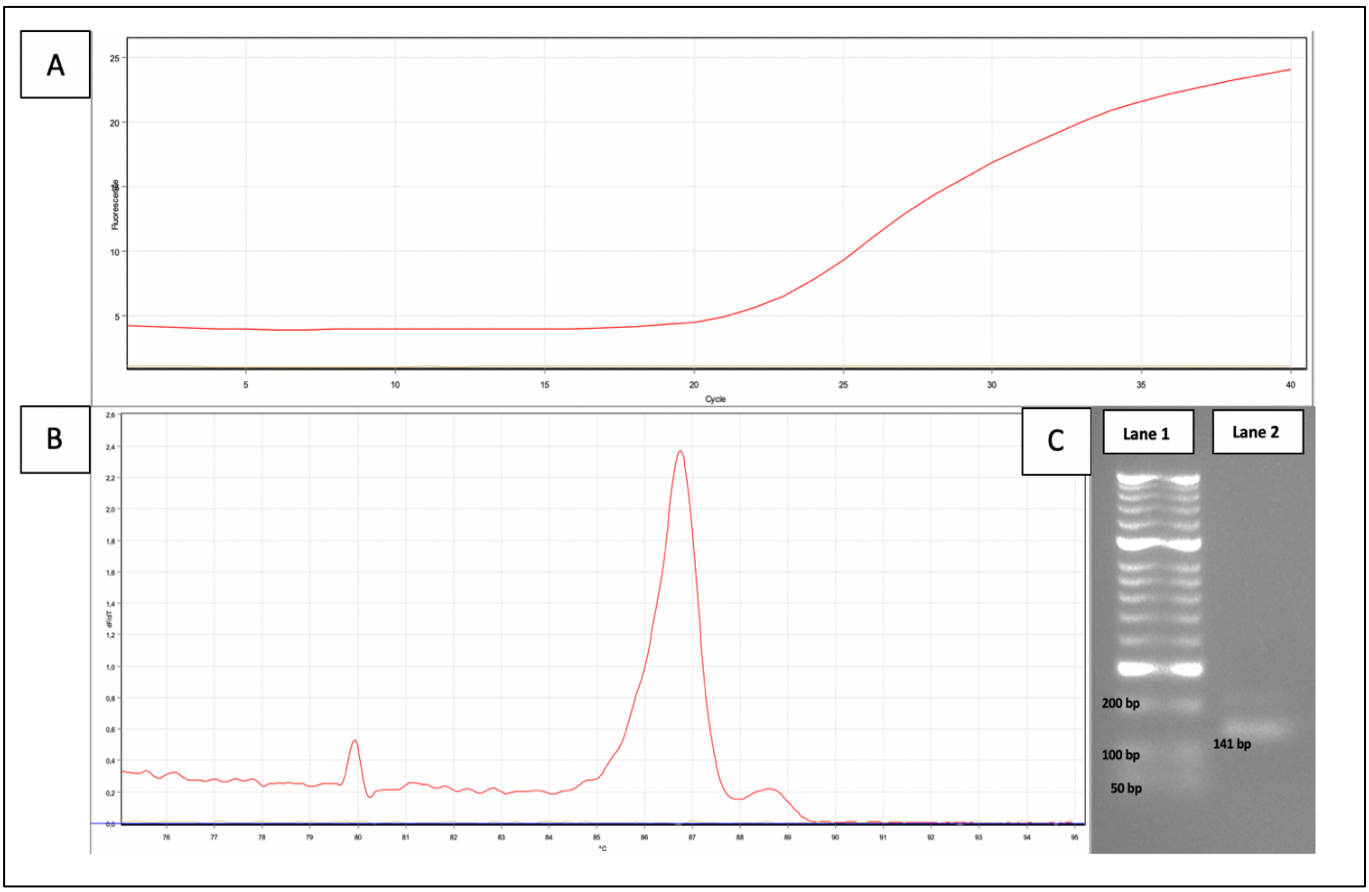

Figure 14 Graphs obtained following HRM with pre-amplification of exon 6

A) The graphical output of the real-time PCR analysis shows amplification on the HRM channel. Fluorescence was detected at approximately 22 cycles, indicated by an increase in the slope of the red line. The slope reaches a plateau at approximately 40 cycles. The NTC is indicated by the flat, yellow line on the graph.

B) The dF/dT vs Temp. curve or the fluorescence melt curve shows a single, tall peak (red line) at approximately 86,5 ºC. This peak indicates the desired PCR product. There is a very small, obscure peak seen to the left of the main peak at approximately 79,8 ºC and a small, 'shoulder' peak is seen on the right-hand side of the main peak. No significant peak is detected in the NTC (yellow line) which eliminates the possible occurrence of reagent contamination.

C) The 2% agarose gel shows a single bright band at the correct product size of 141 bp (lane 2) when compared to the molecular weight marker seen in lane 1. Above the main band, a very faint second band can be seen.

3.3.7 Primer pair 7

By using the optimized PCR conditions, amplification of the target DNA template was achieved for exon 7, as shown in figure 15 below.

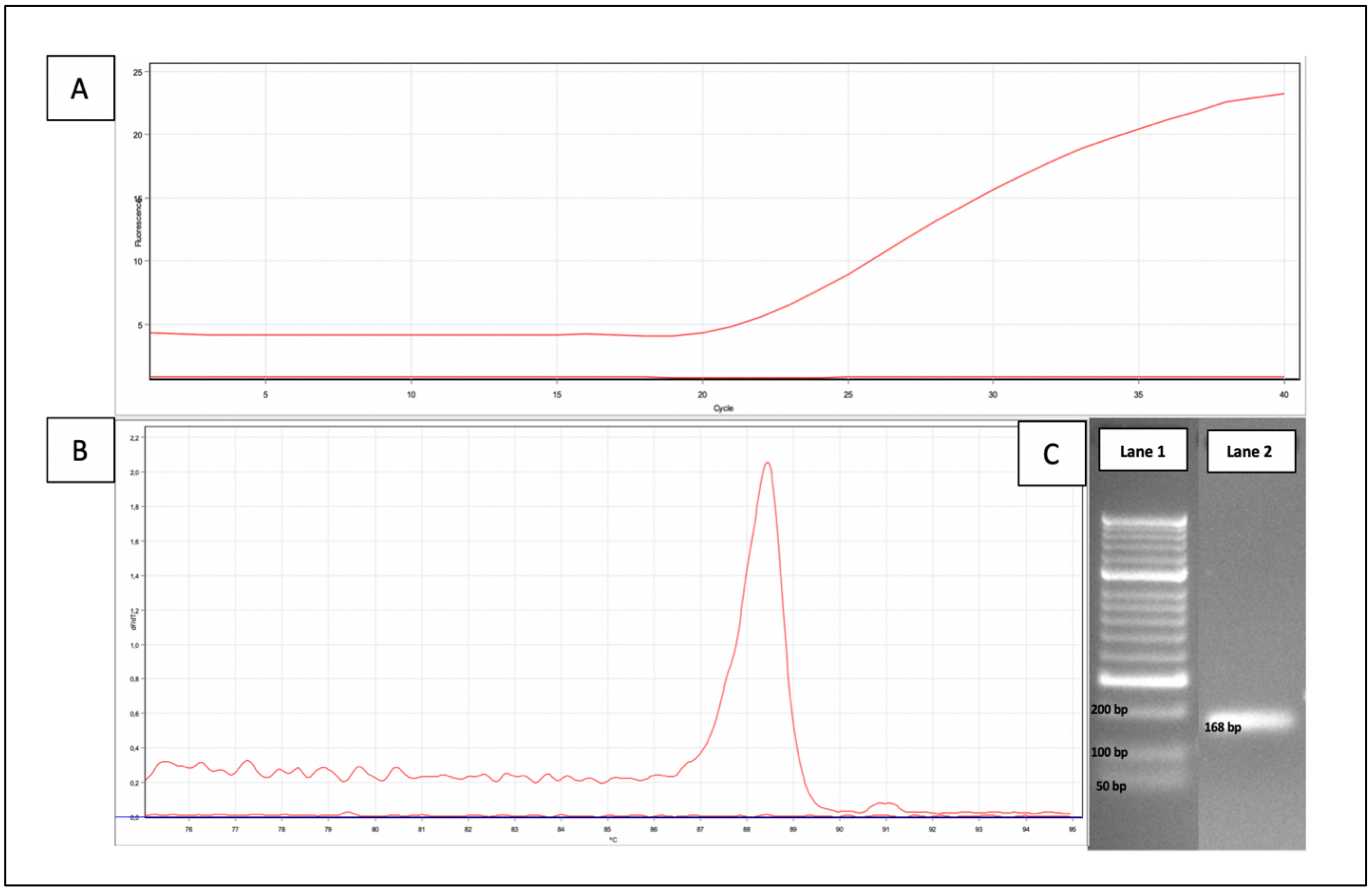

Figure 15 Graphs obtained following HRM with pre-amplification of exon 7

A) The graphical output of the real-time PCR analysis shows amplification on the HRM channel. Fluorescence was detected at approximately 21 cycles, indicated by an increase in the slope of the red line. The slope reaches a plateau at 40 cycles. The NTC is indicated by the orange line on the graph.

B) The dF/dT vs Temp. curve or the fluorescence melt curve shows a single, tall peak (red line) at approximately 88,5 ºC. This peak indicates the desired PCR product. No significant peak is detected in the NTC (orange line) which eliminates the possible occurrence of reagent contamination.

C) The 2% agarose gel shows a single, bright band at the correct product size of 168 bp (lane 2) when compared to the molecular weight marker seen in lane 1.

3.3.8 Primer pair 8

By using the optimized PCR conditions, amplification of the target DNA template was achieved for exon 8, as shown in figure 16 below.

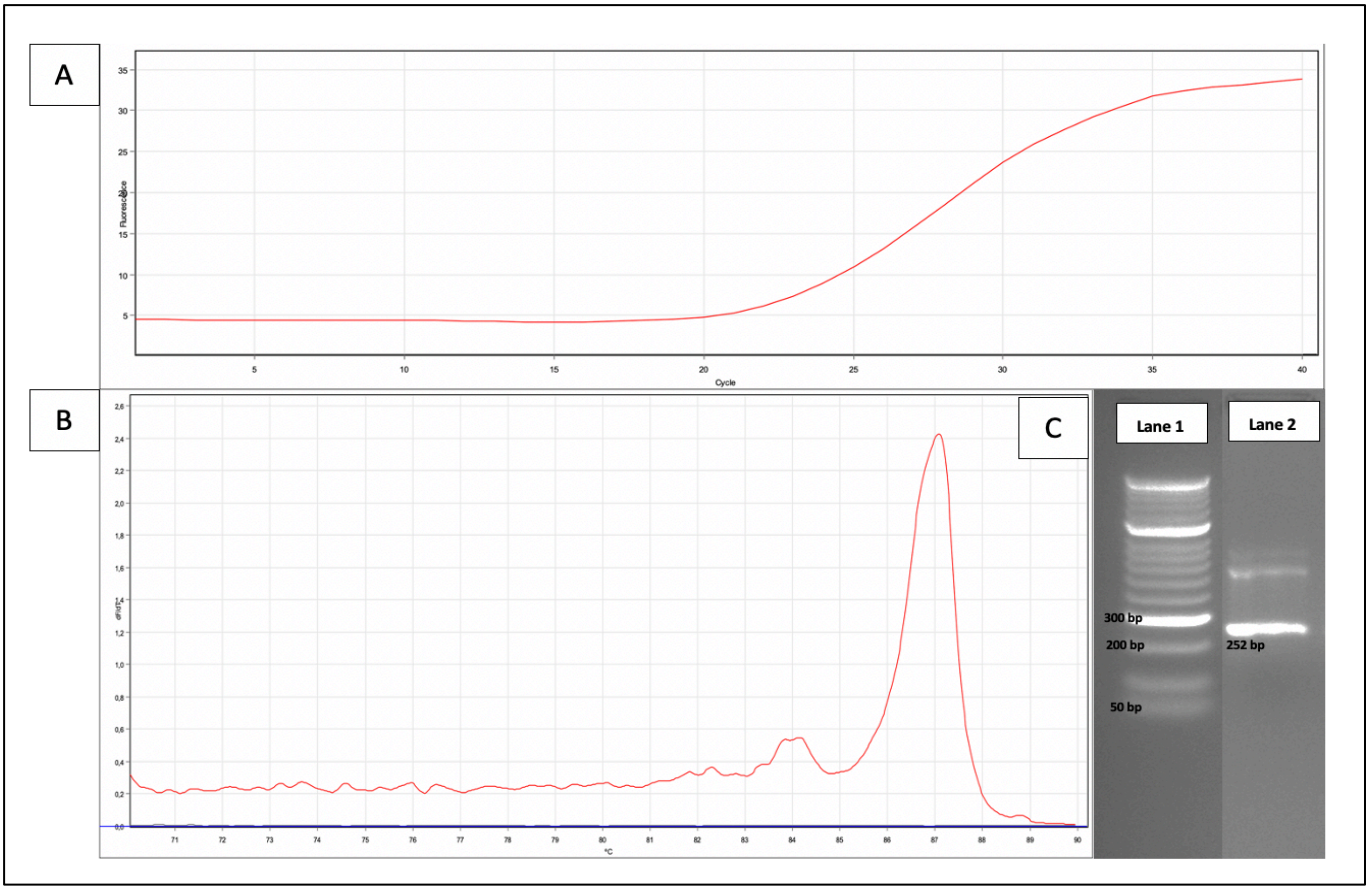

Figure 16 Graphs obtained following HRM with pre-amplification of exon 8.

A) The graphical output of the real-time PCR analysis shows amplification on the HRM channel. Fluorescence was detected at approximately 21 cycles, indicated by an increase in the slope of the red line. The slope reaches a plateau at 40 cycles. The NTC is indicated by the grey line on the graph. The NTC line is not seen on the graph indicating no detection of fluorescence.

B) The dF/dT vs Temp. curve or the fluorescence melt curve shows a single, tall peak (red line) at approximately 87,1 ºC. This peak indicates the desired PCR product. There is a very small, obscure peak seen to the left of the main peak at approximately 84 ºC. No significant peak is detected in the NTC (grey line) which eliminates the possible occurrence of reagent contamination.

C) The 2% agarose gel shows a single bright band at the correct product size of 252 bp (lane 2) when compared to the molecular weight marker seen in lane 1. Above the main band, a faint smear can be seen.

3.3.9 Primer pair 9

By using the optimized PCR conditions, amplification of the target DNA template was achieved for exon 9, as shown in figure 17 below.

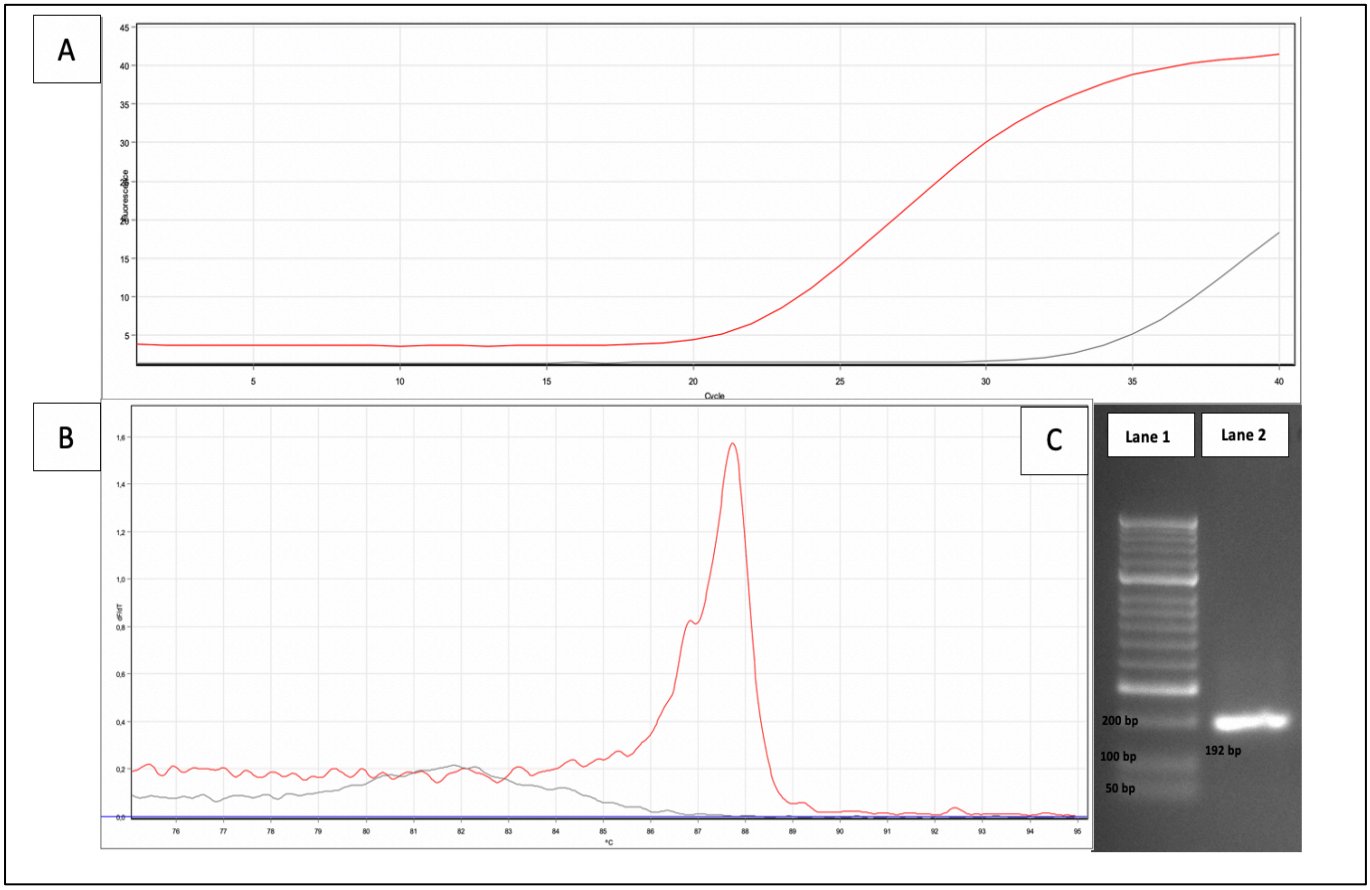

Figure 17 Graphs obtained following HRM with pre-amplification of exon 9.

A) The graphical output of the real-time PCR analysis shows amplification on the HRM channel. Fluorescence was detected at approximately 21 cycles, indicated by an increase in the slope of the red line. The slope reaches a plateau at around 40 cycles. The NTC is indicated by the grey line on the graph. The NTC shows a slight increase in fluorescence, which was detected at approximately 33 cycles.

B) The dF/dT vs Temp. curve or the fluorescence melt curve shows a single, tall peak (red line) at approximately 87,5 ºC. This peak indicates the desired PCR product. A small 'shoulder' peak can be seen on the left-hand side of the peak. No significant peak is detected in the NTC (grey line) which eliminates the possible occurrence of reagent contamination.

C) The 2% agarose gel shows a single, bright band at the correct product size of 192 bp (lane 2) when compared to the molecular weight marker seen in lane 1. Above the main band, a very faint smear can be seen.

3.3.10 Primer pair 10

By using the optimized PCR conditions, amplification of the target DNA template was achieved for exon 10, as shown in figure 18 below.

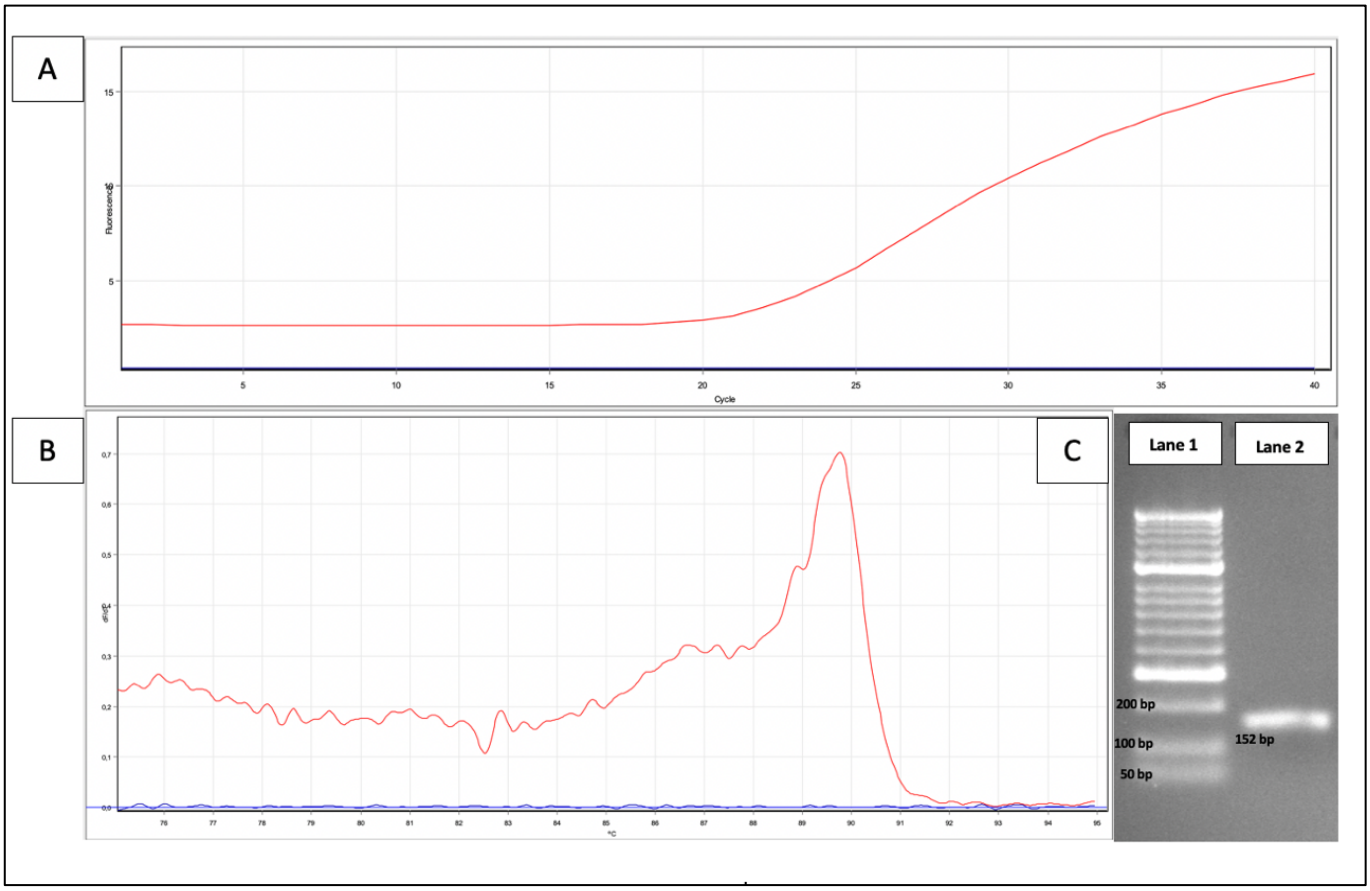

Figure 18 Graphs obtained following HRM with pre-amplification of exon 10.

A) The graphical output of the real-time PCR analysis shows amplification on the HRM channel. Fluorescence was detected at approximately 21 cycles, indicated by an increase in the slope of the red line. The slope reaches a plateau at approximately 40 cycles. The NTC is indicated by the blue line on the graph

B) The dF/dT vs Temp. curve or the fluorescence melt curve shows a single, tall peak (red line) at approximately 89,5 ºC. This peak indicates the desired PCR product. A small 'shoulder' peak can be seen on the left-hand side of the peak and random amplification can be seen preceding the main peak. No significant peak is detected in the NTC (blue line) which eliminates the possible occurrence of reagent contamination.

C) The 2% agarose gel shows a single bright band at the correct product size of 152 bp (lane 2) when compared to the molecular weight marker seen in lane 1.

3.3.11 Primer pair 11

By using the optimized PCR conditions, amplification of the target DNA template was achieved for exon 11, as shown in figure 19 below.

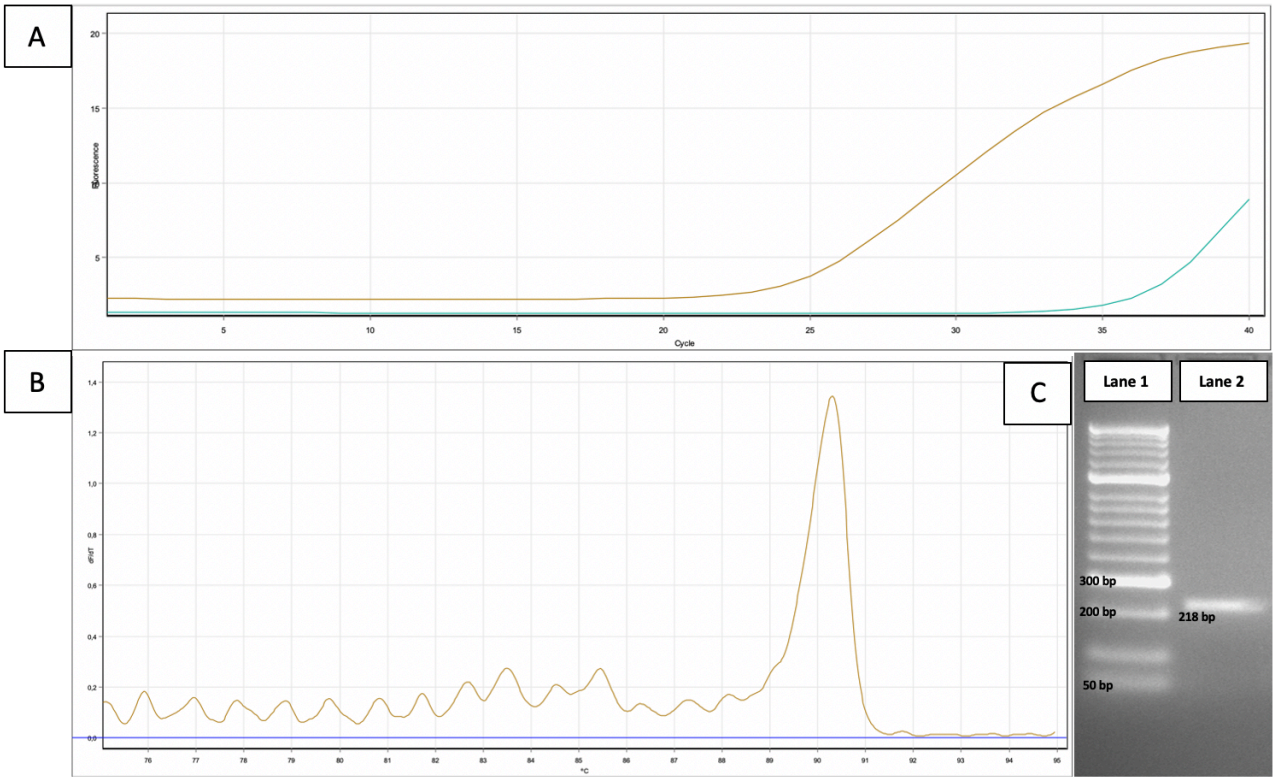

Figure 19 Graphs obtained following HRM with pre-amplification of exon 11.

A) The graphical output of the real-time PCR analysis shows amplification on the HRM channel. Fluorescence was detected at approximately 21 cycles, indicated by an increase in the slope of the red line. The slope reaches a plateau at 40 cycles. The NTC is indicated by the green line on the graph. The NTC shows a slight increase in fluorescence, which was detected at approximately 34 cycles.

B) The dF/dT vs Temp. curve or the fluorescence melt curve shows a single, tall peak (red line) at approximately 90,5 ºC. This peak indicates the desired PCR product. Random amplification can be seen preceding the main peak. No significant peak is detected in the NTC (green line) which eliminates the possible occurrence of reagent contamination.

C) The 2% agarose gel shows a single bright band at the correct product size of 218 bp (lane 2) when compared to the molecular weight marker seen in lane 1.

3.3.12 Primer pair 12

By using the optimized PCR conditions, amplification of the target DNA template was achieved for exon 12, as shown in figure 20 below.

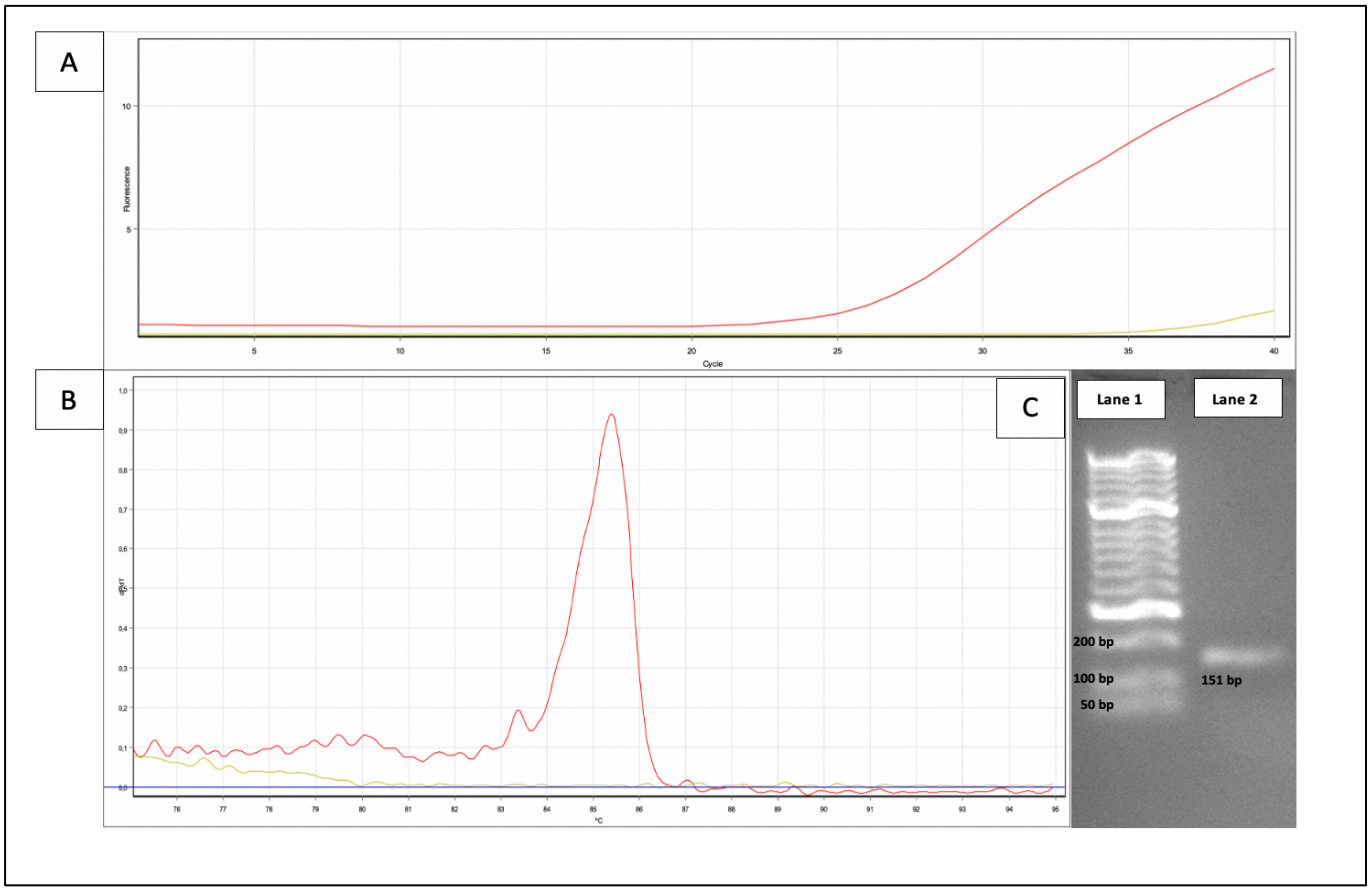

Figure 20 Graphs obtained following HRM with pre-amplification of exon 12.

A) The graphical output of the real-time PCR analysis shows amplification on the HRM channel. Fluorescence was detected at approximately 24 cycles, indicated by an increase in the slope of the red line. The slope reaches a plateau at 40 cycles. The NTC is indicated by the yellow line on the graph. The NTC shows a slight increase in fluorescence, which was detected at 36 cycles.

B) The dF/dT vs Temp. curve or the fluorescence melt curve shows a single, tall peak (red line) at approximately 85,5 ºC. This peak indicates the desired PCR product. A small 'shoulder' peak can be seen on the left-hand side of the peak and random amplification can be seen preceding the main peak. No significant peak is detected in the NTC (yellow line) which eliminates the possible occurrence of reagent contamination.

C) The 2% agarose gel shows a single bright band at the correct product size of 151 bp (lane 2) when compared to the molecular weight marker seen in lane 1.

3.4 HRM real-time PCR analysis

All case samples and control samples were subjected to HRM real-time PCR analysis. The software then grouped case and control samples according to their HRM curve similarities with a confidence interval between 70% - 90%. The resulting groups were displayed in the form of HRM result tables. HRM curve groups, for each exon, and their representative samples are shown in table 11 below.

Table 11 HRM curve groups generated for the 12 exons of the *LMNA* gene and their representative case or control blood samples.

Exon	HRM curve group	Representative sample	Confidence interval (%)
1	1	C2	70
	2	C58	
2	1	R01	70
	2	R05	
	3	C1	
3	1	C63	70
	2	C2	
4	1	C1	70
	2	C10	
	3	C44	
	4	C45	
	5	R010	
5	1	C32	80
	2	R01	
6	1	C1	70
	2	C21	
	3	R01	
	4	C24	
	5	R08	

Exon	HRM curve group	Representative sample	Confidence interval (%)
7	1	C2	80
	2	C3	
	3	C61	
8	1	C1	90
	2	C13	
	3	C44	
	4	C45	
	5	R01	
9	1	C1	70
	2	C3	
	3	C45	
	4	R01	
	5	R06	
10	1	C1	80
	2	C10	
	3	R04	
11	1	C22	75
	2	C10	
	3	R03	
12	1	C1	80
	2	R01	

C = Case blood sample

R= Control blood sample

3.5 Sequencing analysis

Following HRM analysis, representative samples from each HRM group were sent to Inqaba Biotech for Sanger sequencing. The sequencing results were sent back, via email, in the form of chromatograph files which were visualised and analysed using the Unipro Ugene Bioinformatics software. The results obtained following sequencing analysis were as follows:

3.5.1 Exon 1 and Exon 2

The resultant chromatographs from each representative sample of the HRM groups for exon 1 and exon 2 showed clear alignments of the forward and reverse sequence in each sample sequenced. The chromatograph showed no background noise and no trimming of the sequence was necessary. The software detected no ambiguous characters nor any genetic variations in the sequence. No inconsistencies were found when comparing case sample sequences and control sample sequences. Figure 21 below, taken from exon 1- sample 2, is used to demonstrate the sequence alignments for all the representative samples in exon 1 and exon 2.

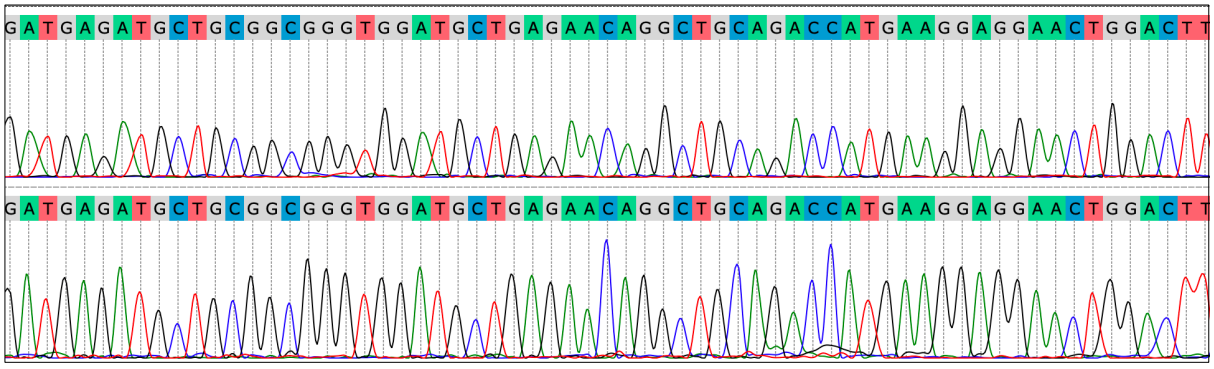

Figure 21 Sequence alignment of exon 1- sample 2 used to demonstrate the sequence alignments for all the representative samples in exon 1 and exon 2.

3.5.2 Exon 3, Exon 6, Exon 8, Exon 9, Exon 10, Exon 11, and Exon 12

The resultant chromatographs from each representative sample of the HRM groups for exons 3, 6, 8, 9, 10, 11, and 12 showed clear alignments of the forward and reverse sequence in each sample sequenced. The chromatograph showed background noise at the starting point and end point of the sequence, therefore, trimming of the sequence was necessary in order to better read the sequence. The software detected no ambiguous characters nor any genetic variations in the sequence. No inconsistencies were found when comparing case sample sequences and control sample sequences. Figure 22 below, taken from exon 3- sample 1, is used to demonstrate the sequence alignments for all the representative samples in exons 3, 6, 8, 9, 10, 11, 12.

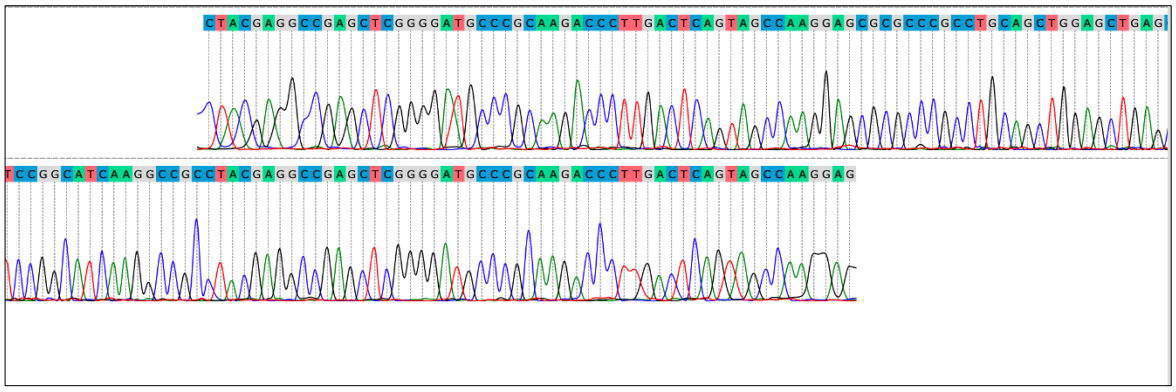

Figure 22 Sequence alignment of exon 3- sample 1 used to demonstrate the sequence alignments for all the representative samples in exon 3, exon 8, exon 9, exon 10 and exon 11.

3.5.3 Exon 4

The resultant chromatographs from each representative sample of the HRM groups for exon 4 showed clear alignments of the forward and reverse sequence in certain samples, specifically case sample 10, case sample 44, case sample 45 and control sample R010. All the resultant chromatographs showed background noise at the starting point and end point of the sequence, therefore, trimming of the sequence was necessary in order to better read the sequence.

In case sample 1, only the forward strand was suitable for analysis and both case sample 10 and case sample 45 showed substantial background noise in the reverse stand causing the software to detect miscalled bases and ambiguous characters (shown as pink blocks on the chromatograph in figure 23) . However, no genetic variations in the sequences were detected. No inconsistencies were found when comparing case sample sequences and control sample sequences. Figure 23 below, taken from exon 4- sample 44, is used to demonstrate the sequence alignments for representative case sample 10, case sample 45 and control sample R010. Figure 24 shows the forward sequence of case sample 1

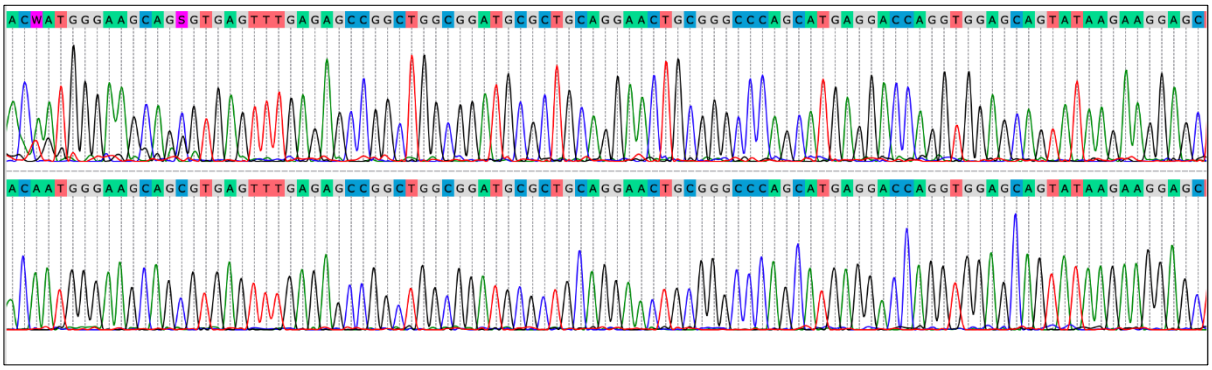

Figure 23 Sequence alignment of exon 4- sample 44, used to demonstrate the sequence alignments for representative case sample 10, case sample 45 and control sample R010.

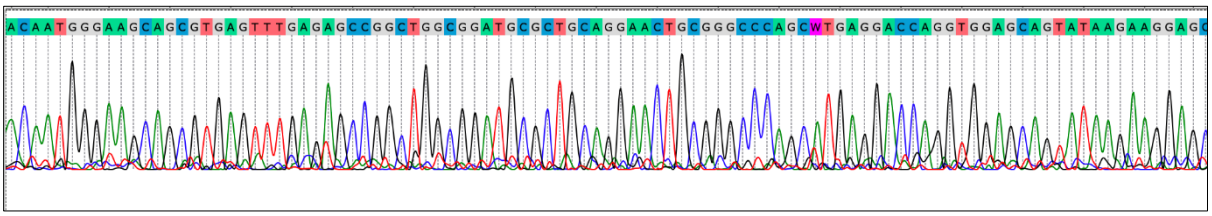

Figure 24 Forward sequence of exon 4 - sample 1

3.5.4 Exon 5

The resultant chromatographs from each representative sample of the HRM groups for exon 5 showed clear alignments of the forward and reverse sequence in each sample sequenced. The chromatograph showed no background noise and no trimming of the sequence was necessary. The software detected a single, homozygous variant at position g.57665 of the reference sequence. The chromatograph shows a substitution variation, in the reverse sequence, where

thymine (T) base was substituted by a cytosine (C) base (T>C). This variant has been previously reported (c.861T>C; p.Ala287; rs538089). This variant was found in case sample 32. The variant was not detected in the control sample 01 (R01), the only other sample sequenced for exon 5. According to the HRM analysis of exon 5, the variant was also detected in case samples 1, 3, 6, 9, 10, 17, 20, 21, 23, 25, 27, 28, 29, 30, 31, 33, 34, 35, 36, 39,40, 41, 42, 43, 44, 45, 46, 47, 49, 51, 52, 54, 55, 56, 57, 59, 60, 63, 64 and 65 as well as control samples R02, R03, R04, R05, R06, R07, R08, R010. Figure 25 below, taken from exon 5- sample 32, shows the substitution variant rs538089.

Figure 25 Substitution variation detected in the reverse sequence of exon 5- sample 32 as aligned to the coding DNA; c.861T>C, p.Ala287 (rs5380809).

3.5.5 Exon 7

The resultant chromatographs from each representative sample of the HRM groups for exon 7 showed clear alignments of the forward and reverse sequence in each sample sequenced. The chromatograph showed no background noise and no trimming of the sequence was necessary. The software detected a single, homozygous variant at position g.58822 of the reference sequence. The chromatograph shows a substitution variation, in the forward sequence, where thymine (T) base was substituted by a cytosine (C) base (T>C). This variant has been previously reported (c.1338T>C; p.Asp446; rs505058). This variant was found in case sample 47. According to the HRM analysis of exon 7, the variant was also detected in case samples 3, 6, 9, 11, 21, 23, 24, 27, 28, 29, 33, 36, 38, 39, 43, 44, 47, 49, 50, 52, 53, 54, 56, 57, 60, 65, 66 as well as control sample R010. Figure 26 below, taken from

exon 7- sample 3, shows the substitution variant rs505058 as aligned to the coding DNA.

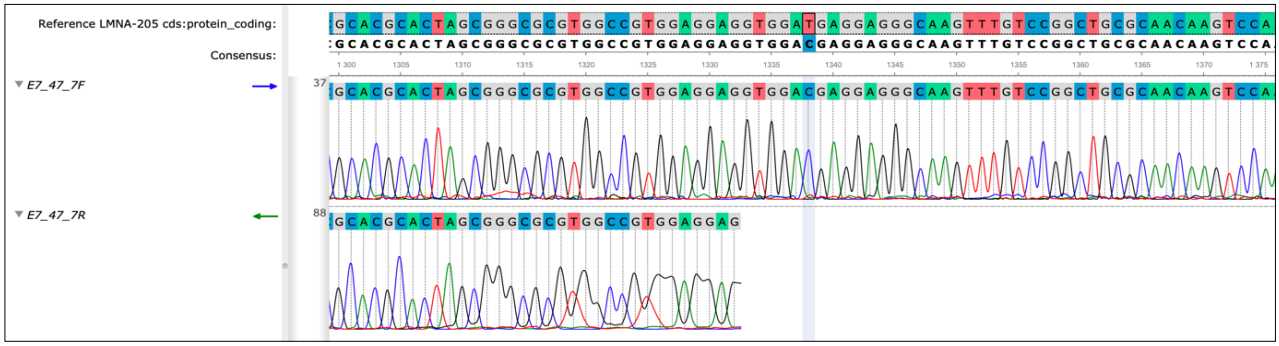

Figure 26 Substitution variation detected in the reverse sequence of exon 7- sample 3 as aligned to the coding DNA; c.1338T>C, p.Asp446 (rs505058).

Chapter 4: Discussion

4.1 The relevance of post-mortem genetic testing of *LMNA* gene variants

Dilated cardiomyopathy is a predominant cause of HF and the most frequent indication for cardiac transplantation, globally (Hitzeroth *et al.*, 2020). This type of CM is also a leading cause of SCD (de Gonzalo-Calvo *et al.*, 2017). It is reported that up to 50% of DCM cases can be attributed to an underlying genetic cause(Fu & Eisen, 2018).

Heart failure is a prevailing form of CVD in SSA and SA (Hitzeroth *et al.*, 2020). Patients suffering from HF in SSA have the highest rate of morbidity and mortality (Noubiap, 2020). The clinical characteristics of HF in SA differ from that in developed countries as (1) it particularly affects younger patients and (2) the causes of HF are mainly non-ischemic (Hitzeroth *et al.*, 2020). Therefore, HF in SA tends to affect economically active adults resulting in a disproportionately negative impact on an already precarious economy (Noubiap, 2020). To date, there is a lack of data on the epidemiology of HF in SA, however, a recent study mentioned by Hitzeroth *et al.* (2020), reported that in 119 acute HF admissions to the Groote Schuur Hospital in Cape Town, DCM was listed as a major cause.

In approximately 40% of DCM patients, a pathogenic variant can be identified as a potential cause of disease (Huang *et al.*, 2020). Pathogenic variants of the *LMNA* gene have been implicated in approximately 6% to 15% of FDCM cases and is the second most common gene associated with FDCM (de Gonzalo-Calvo *et al.*, 2017; Fu & Eisen, 2018). Variants in the *LMNA* gene negatively affect the formation and functioning of Lamin A/C proteins and upset the nuclear membrane stability (Fu & Eisen, 2018). Mounting awareness among cardiologists and geneticists regarding *LMNA* FDCM, has emerged because of the markedly destructive course of the disease in comparison to other inherited CM. This specific cardiac phenotype of *LMNA* pathogenic variants has been associated with a 64% risk of HF development and a 46% risk of SCD (de Gonzalo-Calvo *et al.*, 2017).

This study aimed to identify genetic variants of the *LMNA* gene, in individuals of the South African population, who died suddenly (SUD) due to a suspected SCD. This study forms part of the recommended guidelines from both the European (EHRS) and American Heart Rhythm Societies (AHRS), which states that post-mortem molecular genetic testing should be conducted in cases of SUD, suspected of being due to SCD (Gray *et al.*, 2019).

Post-mortem genetic testing allows researchers to shed light on potentially lethal, underlying genetic disorders, which may remain undiagnosed despite a comprehensive autopsy investigation (Heathfield *et al.*, 2020). It is estimated that 30% of all SD cases, particularly in younger individuals, remain inconclusive even after a complete autopsy investigation as well as other complementary examinations. This is due to the fact that the main cause of SCDY is attributed to inherited structural heart diseases and primary arrhythmogenic disorders (Bagnall *et al.*, 2016), both of which can result in SCD before the development of clear structural changes that can be observed during a conventional autopsy (Gray *et al.*, 2019).

Molecular genetic testing could identify an underlying cardiac disease in 15% to 40% of SD cases and, in combination with clinical screening of family members, may increase the diagnostic yield from 33% to 53% (van den Heuvel *et al.*, 2021). Most genetic cardiac diseases are inherited in a Mendelian fashion, in theory, first-degree family members are at a higher risk of inheriting the same pathogenic variant (Ferrero-Miliani *et al.*, 2010). In this case, molecular genetic testing has dual advantages: (1) it can exclude any non-carriers of causative variants, thereby reducing the number of patients who require follow-up clinical screenings, save much-needed resources in hospitals and ease the minds of family members, and (2) identify carriers of pathogenic variants, whom may have been asymptomatic, and provide potentially life-saving interventions and treatments (Walsh & Cook, 2017). Rather than grappling with a multitude of potential causes left by an inconclusive autopsy, through the use of molecular genetic testing, a precise diagnosis in SCD patients can be achieved (Ferrero-Miliani *et al.*, 2010).

4.2 Primer design and optimisation process

The initial 12 primer pairs (set A), selected for PCR amplification of the *LMNA* gene were sourced from literature (Millat *et al.*, 2009; Taylor *et al.*, 2004). However, following various attempts at PCR optimisation, 7 of the 12 primer pairs were redesigned using the Primer3Web (V4.1.0) software (set B). Primer pair 12 was redesigned once more (set C), due to failed attempts at optimisation.

Optimisation was performed to determine the optimal PCR reaction coditions for correct PCR amplification of the 12 exons of the *LMNA* gene. As per protocol, the primer annealing temperature (T_a) was the first variable altered. Optimised T_as of the primer pairs ranged from 60 ºC to 69 ºC with almost all primers having a T_a above 65 ºC, due to the occurrence of random amplification at lower temperatures. Despite the increased T_a, primer pairs for exon 3 and exon 6 still showed signs of non-specific amplification. After consulting the 'PCR Troubleshooting Guide' from ThermoFisher Scientific, it was decided to shorten the annealing time, from 10 seconds to 8 seconds, to minimise primer binding to non-specific targets. After failed attempts at optimisation using all possible PCR reaction settings, the next variable altered was the primer concentrations. If primer concentrations are too high, nonspecific binding can occur. Primer pairs for exon 3 and exon 11 were optimised at a lower primer concentration of 5 µM.

Amplification of the correct PCR product was confirmed via agarose gel electrophoresis. A bright band, of the correct amplicon size, was visualised for each of the 12 PCR target amplicons. Agarose gel results for primer pairs 2, 3, 4, 6, 8, and 9 showed non-specific binding of primers, in the form of faint secondary bands or smears, despite optimised PCR conditions. This may be due to the poor quality of these primer pairs. The presence of non-specific primer binding did not affect the quality of the melt curve analysis, however, as the correct PCR product was confirmed via Sanger sequencing.

Agarose gel results for primer pairs 1, 5, 10 and 11 showed clear, single bands (of the correct amplicon size) without any secondary bands or smears. However, optimisation results of these primer pairs showed small, secondary peaks on the corresponding

dF/dT vs Temp. curves, indicating random amplification. This may be because of the exceptionally high sensitivity of the RotorGene® Q multiplex HRM thermo cycler machine.

4.3 HRM melt curve analysis of case and control samples

High resolution melt curve analysis is a simple, rapid and inexpensive method that evaluates differences in melt temperatures of targeted PCR amplicons, to detect and identify genetic variants (Chambliss *et al.*, 2017). The RotorGene® Q multiplex HRM platform from (Qiagen, Germany), allows for PCR amplification and high-resolution melt step to be conducted sequentially, on the same thermal cycle instrument, in the same run, which minimizes possible reagent contamination (Chambliss *et al.*, 2017).

Sixty-six case samples and 9 control samples were subjected to real-time PCR amplification followed by HRM curve analysis. The RotorGene® Q multiplex HRM platform (Hilden, Germany) software compared melt curve profiles from case and control samples and grouped them according to their similarities. This grouping was done using a confidence interval threshold range of between 70% and 90%. This lower limit of the confidence interval was selected to account for the high sensitivity of the instrument. Due to the presence of random amplification detected, in certain primer pairs, after PCR optimisation, the RotorGene® Q multiplex HRM platform (Hilden, Germany) software misidentified this non-specific binding as a variation in the sample sequence, resulting in an abnormally high number of samples being tagged as different (or possibly containing variations). Upon sequencing, these samples were found to be the same, with no differences in their sequence. Therefore, the lower limit of 70% for the confidence threshold was selected in order to counteract this sensitivity.

After HRM curve analysis, a total of 40 unique melt curve profiles were detected across all 66 case samples and nine control samples. A single representative sample for each melt curve profile was selected for sequencing via automated Sanger sequencing

4.4 Sequence variant analysis

Two single nucleotide variants (SNVs) of the *LMNA* gene, were identified following Sanger sequencing and sequencing analysis. A missense variant was identified at position g.57665 (position c.861) of the reference sequence. This variant, detected in exon 5, results from the substitution of the thymine nucleotide by a cytosine nucleotide. This variant has been previously reported (c.861T>C; rs538089) and is classified as a benign variant because there is no resulting amino acid change (Gupta *et al.*, 2010; Xie *et al.*, 2015; Zaragoza *et al.*, 2017). This variation occurs at codon 287 and the resulting amino acid remains Alanine (Ala) (p.Ala287, A287A) (figure 4.4.1).

A second missense variant was identified at position g.58822 (position c.1338) in the reference sequence. The variant was detected in exon 7 and is the result of the substitution of the thymine nucleotide by a cytosine nucleotide. This variant has, too, been previously reported (c.1338T>C, rs505058) and is classified as a benign variant (Gupta *et al.*, 2010; Xie *et al.*, 2015; Zaragoza *et al.*, 2017). This variation occurs on the third base of codon 446 and the resulting amino acid remains Aspartic acid (Asp) (p.Asp446, D446D) (figure 27).

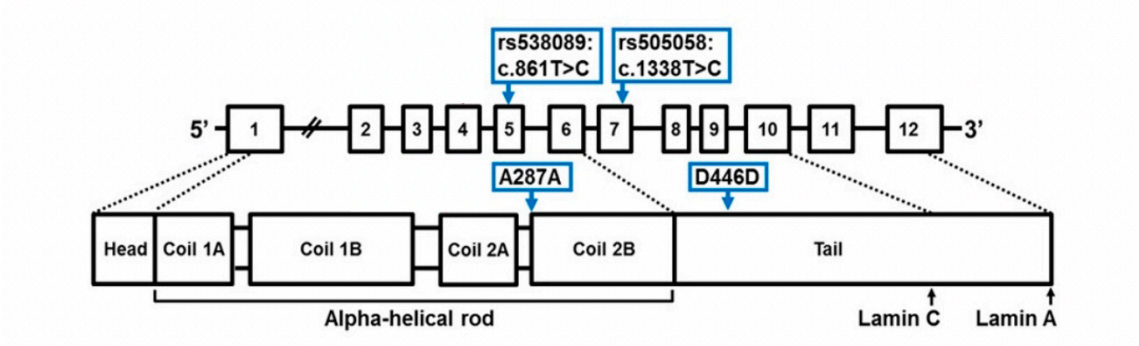

Figure 27 Single nucleotide variants rs535089 (c.861T>C, Ala287Ala) and rs505058 (c.1338T>C, Asp446Asp) in the mRNA and Lamin A/C protein (Zaragoza *et al.*, 2017)

Of the 66 case samples and nine control samples, 46 case samples and eight control samples harbored either one or both of the identified SNVs. Of these, 21 case samples and eight control samples carried only the SNV rs538089, 19 case samples and one control sample carried both SNVs, and six case samples carried only the SNV

rs505058. As is common among *LMNA* genetic variants, the majority of carriers of these SNVs were males (71.7) and of African descent (37/46).

Only the C alleles for each variant (homozygous) was detected in our study population. This is in contrast to other publications which mostly describe these SNVs as heterozygous exonic variants (Zaragoza *et al.*, 2017). It has been reported that these SNVs have a high variant frequency (rs5358089=0.6%; rs505058=0.55%) in all of the available publications (Banerjee *et al.*, 2015; Duesing *et al.*, 2008; Gupta *et al.*, 2010; Méndez-López *et al.*, 2019; Xie *et al.*, 2015; Zaragoza *et al.*, 2017).

These SNVs are commonly described together, in the same publication, and can be found in both case and control groups. Xie *et al.* (2015), identified the SNV rs538089 in nine DCM patients and two control subjects, and the SNV rs505058 in eight DCM patients and three controls subjects. Gupta *et al.* (2010) also reported the detection of both SNVs in the DNA of controls subjects used in the screening of the complete coding sequence plus the intron-exon boundaries of the *LMNA* gene.

4.5 Single nucleotide variations of the *LMNA* gene

Although classified as benign, these SNVs have been associated with various types of laminopathies. In previous reports, both SNVs have been implicated in cases of Werner Syndrome and a sub-type of Charcot-Marie-Tooth Disorder in North-West Africa, both of which are progeroid syndrome laminopathies (Banerjee *et al.*, 2015). Codon 287 (rs5358089) is also associated with a frameshift variation that is reported to cause DCM, therefore a simple variation at this codon could justify an association with DCM (Banerjee *et al.*, 2015) In a study of 78 children with DCM in Children's Hospitals across Shanghai, it was suspected that these SNVs of the *LMNA* gene may be associated with DCM in children (Xie *et al.*, 2015).The SNV rs505058 has also been associated with other diseases such as late-onset Alzheimer's, typically occurring in elderly men, however, more association studies are needed to confirm this (Méndez-López *et al.*, 2019)

4.6 The local relevance of SNVs of the *LMNA* gene

To date, there are no records of these SNVs within the SA population. The NCBI website reports a high alternative C allele frequency of 0.5918 (rs505058) and 0.3998 (rs538089) among the African population. The results generated from this study indicate that these SNVs are common within a SA SCD population but there are no publications that can confirm the association between these SNVs and SCD. An interesting discovery was made in this study, however. In a specific case sample, that of a twenty-nine-year-old, black female, whose cause of death was ruled a SCD secondary to DCM, both the SNVs rs535089 and rs505058 were identified. The relevance of the *LMNA* gene within the SA population is clear, not only for its association with SCD, DCM and HF but with other forms of laminopathy phenotypes that may arise as our population evolves and diversifies.

Chapter 5: Conclusion

The cardiac phenotype of pathogenic *LMNA* variants includes DCM with an aggressive progression to HF and an increased risk of SCD (Gray *et al.*, 2019). These variants tend to affect young, economically active adults and present a unique burden to the local health system and to an already overburdened economy (Shaboodien *et al.*, 2020). Unlike other inherited DCM-associated variants, *LMNA* variants are highly predictable and can be used to confirm diagnosis in carriers.

This study aimed to identify *LMNA* gene variants within a South African SCD population. Two SNVs were identified among both case and control samples used in this study. The SNV rs535089 and SNV rs505058 have been previously identified in other global populations and, as a result of this study, they have now been identified among the South African population. This study was limited by the difficulties of sourcing successful primers from previous literature. There was also a lack of available information regarding the two SNVs we describe in this study. Only six publications made mention of these variants, mainly speculating their association with laminopathy phenotypes.

The identification of these *LMNA* SNVs within the South African population opens a new opportunity for further research into the role of these variants in the development of DCM and HF, two CVDs that severely affect our young population. To date, no single studies on the molecular spectrum have been conducted on the *LMNA* gene in SA. It is clear that there is a need for further research on this gene as our population is moving towards a higher rate of non-communicable diseases, specifically CVDs such as DCM and HF. The inclusion of this gene in the genetic screening of potential at-risk individuals is ideal as pathogenic *LMNA* variants have predictable phenotypes, carriers are likely to experience violent arrhythmias and SCD. These variants are also inherited in a Mandelian pattern, therefore direct family members are at a high risk of disease. The identification of these variants within our population sheds light on how further research is required to fully understand their roles in, not only the development

of DCM and HF, but also in the development of other laminopathies such as EDMD, LGMD, HGPS, Werner Syndrome and Charcot-Marie-Tooth Disorder.

Reference List

Agbor, V. N., Essouma, M., Ntusi, N. A. B., Nyaga, U. F., Bigna, J. J., & Noubiap, J. J. (2018). Heart failure in sub-Saharan Africa: A contemporaneous systematic review and meta-analysis. *Int J Cardiol*, *257*, 207-215. https://doi.org/10.1016/j.ijcard.2017.12.048

Bagnall, R. D., Weintraub, R. G., Ingles, J., Duflou, J., Yeates, L., Lam, L., Davis, A. M., Thompson, T., Connell, V., Wallace, J., Naylor, C., Crawford, J., Love, D. R., Hallam, L., White, J., Lawrence, C., Lynch, M., Morgan, N., James, P., . . . Semsarian, C. (2016). A Prospective Study of Sudden Cardiac Death among Children and Young Adults. *N Engl J Med*, *374*(25), 2441-2452. https://doi.org/10.1056/NEJMoa1510687

Banerjee, A., Ghoshal, P. K., & Sengupta, K. (2015). Novel linkage of LMNA Single Nucleotide Polymorphism with Dilated Cardiomyopathy in an Indian case study. *Int J Cardiol Heart Vasc*, *7*, 99-105. https://doi.org/10.1016/j.ijcha.2015.02.008

Basso, C., Carturan, E., Pilichou, K., Rizzo, S., Corrado, D., & Thiene, G. (2010). Sudden cardiac death with normal heart: molecular autopsy. *Cardiovasc Pathol*, *19*(6), 321-325. https://doi.org/10.1016/j.carpath.2010.02.003

Brown, C. A., Lanning, R. W., McKinney, K. Q., Salvino, A. R., Cherniske, E., Crowe, C. A., Darras, B. T., Gominak, S., Greenberg, C. R., Grosmann, C., Heydemann, P., Mendell, J. R., Pober, B. R., Sasaki, T., Shapiro, F., Simpson, D. A., Suchowersky, O., & Spence, J. E. (2001). Novel and recurrent mutations in lamin A/C in patients with Emery-Dreifuss muscular dystrophy. *Am J Med Genet*, *102*(4), 359-367. https://doi.org/10.1002/ajmg.1463

Burke, M. A., Cook, S. A., Seidman, J. G., & Seidman, C. E. (2016). Clinical and Mechanistic Insights Into the Genetics of Cardiomyopathy. *J Am Coll Cardiol*, *68*(25), 2871-2886. https://doi.org/10.1016/j.jacc.2016.08.079

Campuzano, O., Allegue, C., Partemi, S., Iglesias, A., Oliva, A., & Brugada, R. (2014). Negative autopsy and sudden cardiac death. *Int J Legal Med*, *128*(4), 599-606. https://doi.org/10.1007/s00414-014-0966-4

Captur, G., Arbustini, E., Bonne, G., Syrris, P., Mills, K., Wahbi, K., Mohiddin, S. A., McKenna, W. J., Pettit, S., Ho, C. Y., Muchir, A., Gissen, P., Elliott, P. M., &

Moon, J. C. (2018). Lamin and the heart. *Heart*, *104*(6), 468-479. https://doi.org/10.1136/heartjnl-2017-312338

Caviedes Bottner, P., Córdova Fernández, T., Larraín Valenzuela, M., & Cruces Romero Presentación de Casos Clínicos, P. (2018). Dilated cardiomyopathy and severe heart failure. An update for pediatricians. *Arch Argent Pediatr*, *116*(3), e421-e428. https://doi.org/10.5546/aap.2018.eng.e421 (Miocardiopatía dilatada e insuficiencia cardíaca grave. Puesta al día para el médico pediatra.)

Chambliss, A. B., Resnick, M., Petrides, A. K., Clarke, W. A., & Marzinke, M. A. (2017). Rapid screening for targeted genetic variants via high-resolution melting curve analysis. *Clin Chem Lab Med*, *55*(4), 507-516. https://doi.org/10.1515/cclm-2016-0603

Cimiotti, D., Budde, H., Hassoun, R., & Jaquet, K. (2021). Genetic Restrictive Cardiomyopathy: Causes and Consequences-An Integrative Approach. *Int J Mol Sci*, *22*(2). https://doi.org/10.3390/ijms22020558

Corrado, D., Link, M. S., & Calkins, H. (2017). Arrhythmogenic Right Ventricular Cardiomyopathy. *N Engl J Med*, *376*(1), 61-72. https://doi.org/10.1056/NEJMra1509267

D'Ascenzi, F., Valentini, F., Pistoresi, S., Frascaro, F., Piu, P., Cavigli, L., Valente, S., Focardi, M., Cameli, M., Bonifazi, M., Metra, M., & Mondillo, S. (2022). Causes of sudden cardiac death in young athletes and non-athletes: systematic review and meta-analysis: Sudden cardiac death in the young. *Trends Cardiovasc Med*, *32*(5), 299-308. https://doi.org/10.1016/j.tcm.2021.06.001

De Backer, J., Van Beeumen, K., Loeys, B., & Duytschaever, M. (2010). Expanding the phenotype of sudden cardiac death-An unusual presentation of a family with a Lamin A/C mutation. *Int J Cardiol*, *138*(1), 97-99. https://doi.org/10.1016/j.ijcard.2008.06.008

de Gonzalo-Calvo, D., Quezada, M., Campuzano, O., Perez-Serra, A., Broncano, J., Ayala, R., Ramos, M., Llorente-Cortes, V., Blasco-Turrión, S., Morales, F. J., Gonzalez, P., Brugada, R., Mangas, A., & Toro, R. (2017). Familial dilated cardiomyopathy: A multidisciplinary entity, from basic screening to novel circulating biomarkers. *Int J Cardiol*, *228*, 870-880. https://doi.org/10.1016/j.ijcard.2016.11.045

de Leeuw, R., Gruenbaum, Y., & Medalia, O. (2018). Nuclear Lamins: Thin Filaments with Major Functions. *Trends Cell Biol*, *28*(1), 34-45. https://doi.org/10.1016/j.tcb.2017.08.004

Duesing, K., Charpentier, G., Marre, M., Tichet, J., Hercberg, S., Froguel, P., & Gibson, F. (2008). Evaluating the association of common LMNA variants with type 2 diabetes and quantitative metabolic phenotypes in French Europids. *Diabetologia*, *51*(1), 76-81. https://doi.org/10.1007/s00125-007-0857-z

Fan, L., Yin, P., & Xu, Z. (2022). The genetic basis of sudden death in young people - Cardiac and non-cardiac. *Gene*, *810*, 146067. https://doi.org/10.1016/j.gene.2021.146067

Ferrero-Miliani, L., Holst, A. G., Pehrson, S., Morling, N., & Bundgaard, H. (2010). Strategy for clinical evaluation and screening of sudden cardiac death relatives. *Fundam Clin Pharmacol*, *24*(5), 619-635. https://doi.org/10.1111/j.1472-8206.2010.00864.x

Fu, Y., & Eisen, H. J. (2018). Genetics of Dilated Cardiomyopathy. *Curr Cardiol Rep*, *20*(11), 121. https://doi.org/10.1007/s11886-018-1061-0

Genschel, J., & Schmidt, H. H. (2000). Mutations in the LMNA gene encoding lamin A/C. *Hum Mutat*, *16*(6), 451-459. https://doi.org/10.1002/1098-1004(200012)16:6<451::Aid-humu1>3.0.Co;2-9

Gray, B., Ackerman, M. J., Semsarian, C., & Behr, E. R. (2019). Evaluation After Sudden Death in the Young: A Global Approach. *Circ Arrhythm Electrophysiol*, *12*(8), e007453. https://doi.org/10.1161/circep.119.007453

Gupta, P., Bilinska, Z. T., Sylvius, N., Boudreau, E., Veinot, J. P., Labib, S., Bolongo, P. M., Hamza, A., Jackson, T., Ploski, R., Walski, M., Grzybowski, J., Walczak, E., Religa, G., Fidzianska, A., & Tesson, F. (2010). Genetic and ultrastructural studies in dilated cardiomyopathy patients: a large deletion in the lamin A/C gene is associated with cardiomyocyte nuclear envelope disruption. *Basic Res Cardiol*, *105*(3), 365-377. https://doi.org/10.1007/s00395-010-0085-4

Hammersley, D. J., & Halliday, B. P. (2020). Sudden Cardiac Death Prediction in Non-ischemic Dilated Cardiomyopathy: a Multiparametric and Dynamic Approach. *Curr Cardiol Rep*, *22*(9), 85. https://doi.org/10.1007/s11886-020-01343-9

Heathfield, L. J., Bhengu, W., Louw, S., Martin, L. J., & Ramesar, R. (2020). Assessment of candidate variants causative of inborn metabolic diseases in

SUDI cases in South Africa, and a case report. *Int J Legal Med*, *134*(5), 1639-1645. https://doi.org/10.1007/s00414-020-02337-6

Hitzeroth, J., Mpe, M., Klug, E., Ranjith, N., Sliwa, K., Steingo, L., Lachman, L., Tsabedze, N., Ntusi, N. A. B., & Society Of South Africa, H. F. (2020). 2020 Heart Failure Society of South Africa perspective on the 2016 European Society of Cardiology Chronic Heart Failure Guidelines. *S Afr Med J*, *110*(8b), 13057.

Huang, J., Wan, Q., Zou, Y., Wang, L., & Pan, Y. (2020). Familial dilated cardiomyopathy caused by a novel variant in the Lamin A/C gene: a case report. *BMC Cardiovasc Disord*, *20*(1), 423. https://doi.org/10.1186/s12872-020-01695-8

Jain, A., Norton, N., Bruno, K. A., Cooper, L. T., Jr., Atwal, P. S., & Fairweather, D. (2021). Sex Differences, Genetic and Environmental Influences on Dilated Cardiomyopathy. *J Clin Med*, *10*(11). https://doi.org/10.3390/jcm10112289

Japp, A. G., Gulati, A., Cook, S. A., Cowie, M. R., & Prasad, S. K. (2016). The Diagnosis and Evaluation of Dilated Cardiomyopathy. *J Am Coll Cardiol*, *67*(25), 2996-3010. https://doi.org/10.1016/j.jacc.2016.03.590

Jefferies, J. L., & Towbin, J. A. (2010). Dilated cardiomyopathy. *Lancet*, *375*(9716), 752-762. https://doi.org/10.1016/s0140-6736(09)62023-7

Kang, S. M., Yoon, M. H., & Park, B. J. (2018). Laminopathies; Mutations on single gene and various human genetic diseases. *BMB Rep*, *51*(7), 327-337. https://doi.org/10.5483/bmbrep.2018.51.7.113

Keates, A. K., Mocumbi, A. O., Ntsekhe, M., Sliwa, K., & Stewart, S. (2017). Cardiovascular disease in Africa: epidemiological profile and challenges. *Nat Rev Cardiol*, *14*(5), 273-293. https://doi.org/10.1038/nrcardio.2017.19

Lee, H. H., & Ching, C. K. (2019). Practical Aspects in Genetic Testing for Cardiomyopathies and Channelopathies. *Clin Biochem Rev*, *40*(4), 187-200. https://doi.org/10.33176/aacb-19-00030

Markwerth, P., Bajanowski, T., Tzimas, I., & Dettmeyer, R. (2021). Sudden cardiac death-update. *Int J Legal Med*, *135*(2), 483-495. https://doi.org/10.1007/s00414-020-02481-z

Mayosi, B. M., & Somers, K. (2007). Cardiomyopathy in Africa: heredity versus environment. *Cardiovasc J Afr*, *18*(3), 175-179.

McNally, E. M., & Mestroni, L. (2017). Dilated Cardiomyopathy: Genetic Determinants and Mechanisms. *Circ Res*, *121*(7), 731-748. https://doi.org/10.1161/circresaha.116.309396

Méndez-López, I., Blanco-Luquin, I., Sánchez-Ruiz de Gordoa, J., Urdánoz-Casado, A., Roldán, M., Acha, B., Echavarri, C., Zelaya, V., Jericó, I., & Mendioroz, M. (2019). Hippocampal LMNA Gene Expression is Increased in Late-Stage Alzheimer's Disease. *Int J Mol Sci*, *20*(4). https://doi.org/10.3390/ijms20040878

Millat, G., Chanavat, V., Julia, S., Crehalet, H., Bouvagnet, P., & Rousson, R. (2009). Validation of high-resolution DNA melting analysis for mutation scanning of the LMNA gene. *Clin Biochem*, *42*(9), 892-898. https://doi.org/10.1016/j.clinbiochem.2009.01.016

Mohan, S. B., Parker, M., Wehbi, M., & Douglass, P. (2002). Idiopathic dilated cardiomyopathy: a common but mystifying cause of heart failure. *Cleve Clin J Med*, *69*(6), 481-487. https://doi.org/10.3949/ccjm.69.6.481

Nishiuchi, S., Makiyama, T., Aiba, T., Nakajima, K., Hirose, S., Kohjitani, H., Yamamoto, Y., Harita, T., Hayano, M., Wuriyanghai, Y., Chen, J., Sasaki, K., Yagihara, N., Ishikawa, T., Onoue, K., Murakoshi, N., Watanabe, I., Ohkubo, K., Watanabe, H., . . . Kimura, T. (2017). Gene-Based Risk Stratification for Cardiac Disorders in LMNA Mutation Carriers. *Circ Cardiovasc Genet*, *10*(6). https://doi.org/10.1161/circgenetics.116.001603

Noubiap, J. J. (2020). Tackling heart failure in sub-Saharan Africa: the imperious need for hypertension prevention and control. *Pan Afr Med J*, *36*, 372. https://doi.org/10.11604/pamj.2020.36.372.24528

Peters, S., Johnson, R., Birch, S., Zentner, D., Hershberger, R. E., & Fatkin, D. (2020). Familial Dilated Cardiomyopathy. *Heart Lung Circ*, *29*(4), 566-574. https://doi.org/10.1016/j.hlc.2019.11.018

Rankin, J., & Ellard, S. (2006). The laminopathies: a clinical review. *Clin Genet*, *70*(4), 261-274. https://doi.org/10.1111/j.1399-0004.2006.00677.x

Rosenbaum, A. N., Agre, K. E., & Pereira, N. L. (2020). Genetics of dilated cardiomyopathy: practical implications for heart failure management. *Nat Rev Cardiol*, *17*(5), 286-297. https://doi.org/10.1038/s41569-019-0284-0

Saadi, S., Ben Jomaa, S., Bel Hadj, M., Oualha, D., & Haj Salem, N. (2020). Sudden death in the young adult: a Tunisian autopsy-based series. *BMC Public Health*, *20*(1), 1915. https://doi.org/10.1186/s12889-020-10012-z

Sanchez, O., Campuzano, O., Fernández-Falgueras, A., Sarquella-Brugada, G., Cesar, S., Mademont, I., Mates, J., Pérez-Serra, A., Coll, M., Pico, F., Iglesias, A., Tirón, C., Allegue, C., Carro, E., Gallego, M., Ferrer-Costa, C., Hospital, A., Bardalet, N., Borondo, J. C., . . . Brugada, R. (2016). Natural and Undetermined Sudden Death: Value of Post-Mortem Genetic Investigation. *PLoS One*, *11*(12), e0167358. https://doi.org/10.1371/journal.pone.0167358

Seferović, P. M., Polovina, M., Bauersachs, J., Arad, M., Ben Gal, T., Lund, L. H., Felix, S. B., Arbustini, E., Caforio, A. L. P., Farmakis, D., Filippatos, G. S., Gialafos, E., Kanjuh, V., Krljanac, G., Limongelli, G., Linhart, A., Lyon, A. R., Maksimović, R., Miličić, D., . . . Tschöpe, C. (2019). Heart failure in cardiomyopathies: a position paper from the Heart Failure Association of the European Society of Cardiology. *Eur J Heart Fail*, *21*(5), 553-576. https://doi.org/10.1002/ejhf.1461

Shaboodien, G., Spracklen, T. F., Kamuli, S., Ndibangwi, P., Van Niekerk, C., & Ntusi, N. A. B. (2020). Genetics of inherited cardiomyopathies in Africa. *Cardiovasc Diagn Ther*, *10*(2), 262-278. https://doi.org/10.21037/cdt.2019.10.03

Sliwa, K., Wilkinson, D., Hansen, C., Ntyintyane, L., Tibazarwa, K., Becker, A., & Stewart, S. (2008). Spectrum of heart disease and risk factors in a black urban population in South Africa (the Heart of Soweto Study): a cohort study. *Lancet*, *371*(9616), 915-922. https://doi.org/10.1016/s0140-6736(08)60417-1

Tatli, M., & Medalia, O. (2018). Insight into the functional organization of nuclear lamins in health and disease. *Curr Opin Cell Biol*, *54*, 72-79. https://doi.org/10.1016/j.ceb.2018.05.001

Taylor, M. R., Robinson, M. L., & Mestroni, L. (2004). Analysis of genetic variations of lamin A/C gene (LMNA) by denaturing high-performance liquid chromatography. *J Biomol Screen*, *9*(7), 625-628. https://doi.org/10.1177/1087057104266393

Toit-Prinsloo, D., & Saayman, G. (2012). Performance of autopsies in South Africa: selected legal and ethical perspectives: in South Africa, academic and/or anatomical pathology autopsies are conducted in terms of the Human Tissue Act (Act 65 of 1983).

van den Heuvel, L. M., Do, J., Yeates, L., MacLeod, H., James, C. A., Duflou, J., Skinner, J. R., Semsarian, C., van Tintelen, J. P., & Ingles, J. (2021). Global approaches to cardiogenetic evaluation after sudden cardiac death in the

young: A survey among health care professionals. *Heart Rhythm*, *18*(10), 1637-1644. https://doi.org/10.1016/j.hrthm.2021.03.037

van Deventer, B. S., Rossouw, S. H., & du Toit-Prinsloo, L. (2016). Sudden and unexpected childhood deaths investigated at the Pretoria Medico-Legal Laboratory, South Africa, 2007 - 2011. *SAMJ: South African Medical Journal*, *106*, 983-985. http://www.scielo.org.za/scielo.php?script=sci_arttext&pid=S0256-95742016001000019&nrm=iso

Vimalanathan, A. K., Ehler, E., & Gehmlich, K. (2018). Genetics of and pathogenic mechanisms in arrhythmogenic right ventricular cardiomyopathy. *Biophys Rev*, *10*(4), 973-982. https://doi.org/10.1007/s12551-018-0437-0

Walsh, R., & Cook, S. A. (2017). Issues and Challenges in Diagnostic Sequencing for Inherited Cardiac Conditions. *Clin Chem*, *63*(1), 116-128. https://doi.org/10.1373/clinchem.2016.254698

Xie, L. J., Xiao, T. T., Huang, M., & Shen, J. (2015). LMNA gene single nucleotide polymorphisms in dilated cardiomyopathy of Han children. *Int J Clin Exp Med*, *8*(7), 11230-11234.

Zaragoza, M. V., Nguyen, C. H. H., Widyastuti, H. P., McCarthy, L. A., & Grosberg, A. (2017). Dupuytren's and Ledderhose Diseases in a Family with LMNA-Related Cardiomyopathy and a Novel Variant in the ASTE1 Gene. *Cells*, *6*(4). https://doi.org/10.3390/cells6040040

Appendix A: Certificate of ethical clearance

UNIVERSITEIT VAN PRETORIA
UNIVERSITY OF PRETORIA
YUNIBESITHI YA PRETORIA

Faculty of Health Sciences

Institution: The Research Ethics Committee, Faculty Health Sciences, University of Pretoria complies with ICH-GCP guidelines and has US Federal wide Assurance.

- FWA 00002567, Approved dd 18 March 2022 and Expires 18 March 2027.
- IORG #: IORG0001762 OMB No. 0990-0278 Approved for use through August 31, 2023.

Faculty of Health Sciences **Research Ethics Committee**

12 August 2022

Approval Certificate
Annual Renewal

Dear Miss NM Da Silva,

Ethics Reference No.: 373/2021 – Line 1
Title: Genetic analysis of Lamin A/C gene variants in cases of sudden cardiac death admitted to a medico-legal laboratory

The **Annual Renewal** as supported by documents received between 2022-07-13 and 2022-08-10 for your research, was approved by the Faculty of Health Sciences Research Ethics Committee on 2022-08-10 as resolved by its quorate meeting.

Please note the following about your ethics approval:

- Renewal of ethics approval is valid for 1 year, subsequent annual renewal will become due on 2023-08-12.
- Please remember to use your protocol number (373/2021) on any documents or correspondence with the Research Ethics Committee regarding your research.
- Please note that the Research Ethics Committee may ask further questions, seek additional information, require further modification, monitor the conduct of your research, or suspend or withdraw ethics approval.

Ethics approval is subject to the following:

- The ethics approval is conditional on the research being conducted as stipulated by the details of all documents submitted to the Committee. In the event that a further need arises to change who the investigators are, the methods or any other aspect, such changes must be submitted as an Amendment for approval by the Committee.

We wish you the best with your research.

Yours sincerely

On behalf of the FHS REC, Dr R Sommers
MBChB, MMed (Int), MPharmMed, PhD
Deputy Chairperson *of the Faculty of Health Sciences Research Ethics Committee, University of Pretoria*

The Faculty of Health Sciences Research Ethics Committee complies with the SA National Act 61 of 2003 as it pertains to health research and the United States Code of Federal Regulations Title 45 and 46. This committee abides by the ethical norms and principles for research, established by the Declaration of Helsinki, the South African Medical Research Council Guidelines as well as the Guidelines for Ethical Research: Principles Structures and Processes, Second Edition 2015 (Department of Health)

Research Ethics Committee
Room 4-60, Level 4, Tswelopele Building
University of Pretoria, Private Bag x323
Gezina 0031, South Africa
Tel +27 (0)12 356 3084
Email: deepeka.behari@up.ac.za
www.up.ac.za

Fakulteit Gesondheidswetenskappe
Lefapha la Disaense tša Maphelo

Appendix B: DNA extraction process

Preceding the DNA extraction process, the wash buffers, provided in the new kit, were prepared. To the 98 mL buffer AW1 (wash buffer Ⅰ) concentrate, 130 mL of ethanol (100%) was added. Similarly, 160 mL of ethanol (100%) was added to the 66 mL buffer AW2 (wash buffer Ⅱ) concentrate. The bottle caps, on each bottle, were tightly fastened and the bottles were shaken, thoroughly, by hand, to ensure that the ethanol was well incorporated into the wash buffer concentrates. Completion of this step was indicated by marking the bottle caps, on each of the wash buffer bottles, with a small cross.

Before initiating the DNA extraction process, the orbital incubator, located within the chemical pathology laboratory, was switched on and heated to a temperature of 56 ºC. The workbench, where the extraction process took place, as well as all the equipment (microcentrifuge tube racks, pipettes, etc.) used were sanitized to prevent any possible contamination. All standing reagent bottles were mixed, by hand, to eliminate possible precipitates, which may have formed within the solutions. Whole-blood samples, that were used in the extraction process, were retrieved from the freezer, and were allowed to thaw, completely, before the initial step of the extraction protocol.

The extraction of genomic DNA from a single, whole-blood sample, began as follows: A volume of 20 μL of Qiagen Protease or Protease K was pipetted into a 1.5 mL microcentrifuge tube. Protease K was used to initiate degradation of the nucleus, releasing the nucleic acids, and aided in protecting the nucleic acids from nuclease attack. Thereafter, 200 μL of whole-blood was pipetted into the 1.5 mL microcentrifuge tube. Once the protease K and the whole-blood were mingled, 200 μL of buffer AL or lysis buffer was pipetted into the microcentrifuge tube. The lysis buffer resulted in the lysis of the cellular membranes, within the whole-blood. After this, the 1.5 mL microcentrifuge tube was pulse-vortexed for 15 seconds, to ensure that the contents of the tube were sufficiently amalgamated.

The 1.5 mL microcentrifuge tube was then placed into the preheated, orbital incubator. The tube was incubated at 56 ºC for ten minutes, thereafter, the tube was removed from the incubator, pulse-vortexed, and returned to the incubator for another 10

minutes. This incubation process was repeated exactly three times, increasing the incubation time to 30 minutes. This additional step was suggested as a troubleshooting method, stated in the extraction protocol, to ensure sufficient lysis of cellular structures and to allow the complete release of nucleic acids. Once the incubation time had ended, the tube was removed from the incubator and centrifuged, briefly, to remove droplets that may have settled on the inside of the tube lid or the sides of the microcentrifuge tube. Following this, 200 μL of ethanol (100%) was pipetted into the tube and the tube was, once again, pulse-vortexed for approximately 15 seconds and, subsequently centrifuged for a few seconds, to remove any displaced droplets within the tube. The succeeding step involved preparing the QIAamp mini spin column, by placing the mini spin column into a 2 mL collection tube. Both the QIAamp mini spin column and the 2 mL collection tube were provided in the QIAamp DNA mini blood kit (50) (Qiagen, Germany).

The contents of the 1.5 mL microcentrifuge tube were then transferred into the QIAamp mini spin column. The spin column, consisting of the mini spin column within the 2 mL collection tube, was centrifuged at 6000 x g for approximately one minute. Thereafter, the filtrate collected in the 2 mL collection tube was discarded into a biohazard waste bin and the mini spin-column was transferred to a new, clean 2 mL collection tube.

Next, 500 μL of buffer AW1 solution was pipetted into the mini-spin column. The spin-column was then centrifuged at 6000 x g for one minute and 30 seconds. The addition of half a minute, to the centrifugation time suggested by the extraction protocol, was yet another troubleshooting method used to ensure proper filtration through the silica membrane. Once again, the resulting filtrate, within the collection tube, was discarded and the mini spin-column was transferred to a new, clean 2 mL collection tube. Following this, 500 mL of buffer AW 2 was pipetted into the mini spin column. The spin-column was then centrifuged at full speed (20 000 x g) for three minutes.

The penultimate step of the extraction process involved transferring the mini spin-column to a new, clean 1.5 mL microcentrifuge tube. A volume of 200 μL of buffer AE (elution buffer) solution was added into the mini spin-column. This volume was adjusted, and less elution buffer solution was used to produce a more concentrated

DNA solution. The buffer AE solution was pipetted into the center of the membrane, located within the mini spin-column. Special care was taken to ensure that the pipette tip did not touch the silica membrane. The mini spin-column and the elution buffer were allowed to stand, at room temperature (19 ºC- 25 ºC), for approximately two minutes. This was done to allow the elusion buffer to completely infiltrate the silica membrane. Buffer AE is a low salt solution used to elute DNA bound to the silica membrane. The rehydration of the bound DNA and the membrane surface results in the unbounding of the DNA from the membrane and allows the DNA to flow out during the following centrifugation step. The spin column, consisting of the mini spin column within the 1.5 mL microcentrifuge tube, was centrifuged at full speed (20 000 x g) for one minute and 30 seconds.

Finally, the mini spin-column was removed from the 1.5 mL microcentrifuge tube and discarded into a biohazard waste bin. Immediately after, the microcentrifuge tube, containing the purified DNA solution, was sealed, and labeled according to the corresponding sample number.

Appendix C: Tris-acetate-EDTA (TAE) buffer

1. Prepare 800 mL of dH2O in a suitable container.
2. Add 242 g of Tris base to the solution.
3. Add 18.61 g of Disodium EDTA to the solution.
4. Add 59.955 g of Acetic Acid to the solution.
5. The 1x TAE solution is 40mM Tris, 20mM Acetate and 1mM EDTA and typically has a pH around 8.6 (do not adjust).
6. Add dH2O until the volume is 1 L.

Appendix D: Individual DNA concentrations and purity ratios for all case and control samples

Case Samples

Case sample number	DNA concentration (μg/mL)	Purity (λ 260/280)	Absorbance (λ260/320)
1	(i) 54,092	1,891	2,237
	(ii) 188,68	1,070	3,306
2	24,421	1,909	2,343
3	76,259	1,940	2,376
4	17,101	2,027	2,324
5	63,124	1,947	2,163
6	26,205	1,947	2,127
7	112,81	2,009	2,189
8	107,90	2,007	2,181
9	11,809	1,988	2,399
10	(i) 21,607	1,901	2,139
	(ii) 158,93	1,932	1,925
11	11,497	2,036	2,476
12	15,211	1,994	2,260
13	69,812	1,951	2,269
14	12,077	1,953	2,317
15	12,744	1,820	1,977
16	(i) 9,178	1,857	1,878
	(ii) 66,375	1,883	1,034

17	15,118	2,022	2,191
18	15,874	1,939	2,277
19	22,896	1,992	2,279
20	17,432	1,951	2,335
21	(i) 19,924	1,865	1,500
	(ii) 95,868	1,897	1,914
22	35,716	1,907	2,236
23	13,890	1,892	2,130
24	(i) 18,871	1,941	1,895
	(ii) 150,73	1,684	1,902
25	16,984	1,958	2,482
26	(i) 35,942	1,988	2,161
	(ii) 168,74	1,990	1,942
27	32,574	1,936	2,344
28	16,758	1,966	2,684
29	8,628	1,939	1,699
30	38,214	1,955	2,272
31	12,026	1,944	2,101
32	15,174	1,846	1,476
33	(i) 75,970	1,872	1,386
	(ii) 47,796	1,805	1,086
34	(i) 18,032	1,884	2,194
	(ii) 114,97	1,949	1,523
35	(i) 13,003	1,884	2,194
	(ii) 72,735	1,845	1,796
36	(i) 25,871	1,915	2,175
	(ii) 140,38	1,950	1,450

37	(i) 44,666	1,931	2,255
	(ii) 133,45	1,843	1,826
38	(i) 11,473	1,848	2,060
	(ii) 78,512	1,760	0,909
39	(i) 43,093	1,948	2,297
	(ii) 221,66	1,893	1,607
40	(i) 18,970	1,844	1,991
	(ii) 77,806	1,918	1,068
41	(i) 92,663	1,934	2,288
	(ii) 147,34	1,918	
42	(i) 54,201	1,955	2,293
	(ii) 253,65	1,830	1,309
43	(i) 32,262	1,958	2,205
	(ii) 108,19	1,926	1,719
44	(i) 96,856	1,868	1,072
	(ii) 69,04	1,835	0,882
45	(i) 33,468	1,930	2,039
	(ii) 177,46	1,849	1,800
46	(i) 61,138	1,945	2,076
	(ii) 207,77	1,980	1,799
47	(i) 19,765	1,981	2,291
	(ii) 122,87	1,764	1,559
48	28,532	1,937	2,132
49	(i) 13,064	1,948	1,831
	(ii) 68,105	1,954	1,598
50	(i) 25,821	2,020	2,137
	(ii) 105,53	2,007	2,012
51	11,995	1,883	1,289
52	12,800	1,804	1,114
53	16,036	1,879	1,249

54	12,390	1,862	0,971
55	23,172	1,959	1,709
56	30,224	1,885	2,257
57	11,640	1,965	1,362
58	21,104	1,916	2,008
59	25,512	1,930	2,074
60	11,919	1,881	1,105
61	12,241	1,827	0,978
62	8,069	1,855	0,913
63	22,234	1,920	2,108
64	32,781	1,876	1,880
65	26,123	1,803	1,311
66	25,895	1,934	1,333
(i)- First extraction (ii)- Second extraction			

Control samples

Control sample number	**DNA concentration (µg/mL)**	**Purity (λ 260/280)**	**Absorbance (λ260/320)**
R01	(i) 33,874	2,136	1,539
	(ii) 35,27	1,603	1,072
R02	14,106	2,034	1,355

R03	26,148	1,959	2,325
R04	15,316	3,070	1,114
R05	52,329	1,825	0,960
R06	11,753	2,903	0,663
R07	13,746	1,947	-1,900
R08	135,070	1,987	0,865
R010	33,848	1,907	2,229
(i)- First extraction (ii)- Second extraction			